

Distinct signatures of spinning PBH domination and evaporation: *doubly peaked gravitational waves, dark relics and CMB complementarity*

Nilanjandev Bhaumik  *, Anish Ghoshal  †, Rajeev Kumar Jain  * and Marek Lewicki  †

*Department of Physics, Indian Institute of Science, Bangalore 560012, India

†Institute of Theoretical Physics, Faculty of Physics, University of Warsaw,
ul. Pasteura 5, 02-093 Warsaw, Poland

E-mail: nilanjandev@iisc.ac.in, anish.ghoshal@fuw.edu.pl, rkjain@iisc.ac.in,
marek.lewicki@fuw.edu.pl

Abstract. Ultra-low mass primordial black holes (PBH), which may briefly dominate the energy density of the universe but completely evaporate before the big bang nucleosynthesis (BBN), can lead to interesting observable signatures. In our previous work, we studied the generation of a doubly peaked spectrum of induced stochastic gravitational wave background (ISGWB) for such a scenario and explored the possibility of probing a class of baryogenesis models wherein the emission of massive unstable particles from the PBH evaporation and their subsequent decay contributes to the matter-antimatter asymmetry. In this work, we extend the scope of our earlier work by including spinning PBHs and consider the emission of light relativistic dark sector particles, which contribute to the dark radiation (DR) and massive stable dark sector particles, thereby accounting for the dark matter (DM) component of the universe. The ISGWB can probe the non-thermal production of these heavy DM particles, which cannot be accessible in laboratory searches. For the case of DR, we find a novel complementarity between the measurements of ΔN_{eff} from these emitted particles and the ISGWB from PBH domination. Our results indicate that the ISGWB has a weak dependence on the initial PBH spin. However, for gravitons as the DR particles, the initial PBH spin plays a significant role, and only above a critical value of the initial spin parameter a_* , which depends only on initial PBH mass, the graviton emission can be probed in the CMB-HD experiment. Upcoming CMB experiments such as CMB-HD and CMB-Bharat, together with future GW detectors like LISA and ET, open up an exciting possibility of constraining the PBHs parameter space providing deeper insights into the expansion history of the universe between the end of inflation and BBN.

Keywords: Primordial black holes, Stochastic gravitational wave background, Baryogenesis, CMB, Dark matter, Dark radiation

Contents

1	Introduction	1
2	Spinning PBHs, their evaporation, and the background evolution	3
3	Induced stochastic gravitational wave background (ISGWB) from spinning PBHs	6
4	Signatures of spinning PBHs in different scenarios	10
4.1	Dark radiation	10
4.2	Dark matter relic density	15
4.3	Baryogenesis	19
5	Conclusions and discussions	22

1 Introduction

The idea of primordial black holes (PBH) was first put forward by Zel’dovich and Novikov [1], and later studied in depth by Hawking and Carr [2–4]. The formation of PBHs in the very early universe has different interesting implications for both cosmology and particle physics [5–7]. On the one hand, in the present cosmological landscape of various dark matter (DM) candidates, PBHs have emerged as an important candidate for the cold DM due to the possibility of testing their signatures in gravitational wave (GW) detectors [8–14]. Though the abundance of PBHs is strongly constrained in different mass ranges [7, 15–31], there remains an open window in the asteroid mass range ($10^{-16} - 10^{-14} M_{\odot}$) wherein PBHs can be the entire DM [32]. On the other hand, the possibility of PBH formation in the post inflationary universe due to the amplified inflationary scalar perturbations (for example, from ultra-slow-roll models of inflation [33–38], warm inflation [39–41], Gauss-Bonnet theories of inflation [42], two-field models of inflation [43–45] etc.) has opened up an interesting avenue to constrain the inflationary perturbations modes leaving horizon during last forty e-folds of inflation. In such a scenario, PBHs can help in probing the cosmic history between the end of inflation to the start of the Big Bang Nucleosynthesis (BBN), which is not accessible by any other direct observational probes. PBHs have also been suggested to form from strong first-order phase transitions in early universe [46–49], the collapse of topological defects [50–55], scalar condensates and topological and non-topological solitons [56], resonant reheating [57], preheating [58–61] and confinement of quarks [62]. Thus PBHs can help probe or potentially constrain these scenarios. Here we focus on various signatures of ultra-low mass PBHs ($M_{\text{PBH}} \lesssim 10^9 \text{ g}$), and how future GW and CMB probes can constrain PBHs parameter space as well as cosmological history before BBN, through these signatures.

Smaller mass PBHs evaporate much faster. As a result, PBHs with mass $M_{\text{PBH}} \lesssim 10^{-18} M_{\odot}$ ($M_{\text{PBH}} \lesssim 10^{15} \text{ g}$) would be completely evaporated by today. BBN provides stringent constraints on the abundance of PBHs in the early universe for masses $10^9 \text{ g} \leq M_{\text{PBH}} \leq 10^{14} \text{ g}$ [16, 63, 64], as PBHs of this mass range evaporates during or after BBN. On the other hand, PBHs with mass below 10^9 g evaporate far before BBN. Therefore, if formed with appropriate abundance, they can dominate the universe’s energy density for a short

duration before their evaporation. This window reveals the possibility that PBHs may have dominated the early universe before BBN and played an important role in its evolution. The consequences of an early PBH-dominated epoch have been well studied since the Hawking evaporation of PBHs involves many different and important aspects, for instance, the generation of Dark Radiation (DR) [65–70], matter-antimatter asymmetry production [71–80], and the implications for the production of DM through evaporation [66, 68, 69, 72, 81–93].

The imprints of PBHs on the induced stochastic gravitational wave background (ISGWB) can be broadly classified into a few categories according to their origin. One is from the binary mergers of the PBHs [94–99], which can be produced even in the very late universe. Another class of ISGWB comes from the second-order tensor perturbations, which is related to the formation mechanism of PBHs [100–106]. Moreover, the gravitons produced during Hawking evaporation of PBHs can also contribute to the GWs but at a very high frequency ($10^{13} - 10^{16}$ Hz), which makes this source difficult to detect [107]. The scenario we had focused on in our earlier work [80] is slightly different from these popular classes of PBH-GW associations. We focused on the resonant contributions [108] of the second-order tensor perturbations from two different origins of adiabatic scalar perturbations. The first one directly comes from the inflationary adiabatic perturbations [109], while the second is induced by the isocurvature perturbations from the PBHs population of monochromatic [80, 110–112] or extended mass distribution [113]. In this scenario, we found a distinctive doubly-peaked spectral shape of the ISGWB.

Our previous work considered only the Schwarzschild PBHs without any spin. In this work, we extend the scope of our study by including the possibility of initially spinning PBHs. We studied the case of Hawking-evaporation-driven baryogenesis in our previous work. Here we consider a broader class of possible phenomena associated with an early ultra-low mass PBH-dominated universe, connect them with the associated ISGWB signatures, and look for different effects from spinning PBHs. During their evaporation, PBHs can emit both relativistic and massive non-relativistic particles. If the emitted relativistic particles belong to the dark sector, they can contribute to the universe’s total radiation energy density, usually referred to as DR. It can be characterized by an effective number of neutrinos, ΔN_{eff} and can be constrained during the CMB era with current and future CMB probes or during the BBN epoch. This offers a complementary probe for our scenario besides the corresponding ISGWB. One interesting point to note here is that ISGWB also contributes to radiation energy density and, therefore, to ΔN_{eff} . While this ISGWB contribution to ΔN_{eff} is generic to the scenario of PBH domination, the dark radiation is a special case when we consider some particular DR particles. Therefore the resulting DR can be constrained in three different channels, DR- ΔN_{eff} in CMB observations, ISGWB- ΔN_{eff} in CMB observations and the detection of ISGWB signals in the future GW observatories.

Massive non-relativistic particles from Hawking evaporation can decay in a baryon-number violating process and contribute to baryogenesis. In the same context, it is possible to consider stable non-relativistic particles in the dark sector. They can constitute the observed DM energy density if they do not decay. Detection or non-detection of doubly peaked ISGWB spectrum can also very effectively constrain the parameter space for this DM production mechanism. Thus, in this work, we connect the generation of DR and DM from PBH evaporation with corresponding ISGWB signals. We also explore whether initially spinning PBHs would leave a distinct signature, allowing us to determine the spin of these black holes. For the ISGWB sector, we find the effect of initial PBH spin to be non-zero but small. When we consider non-relativistic particles with spin ≤ 1 contributing to baryogenesis

and DM relic density, we find a negligible effect of the initial PBH spin. The situation changes only when we consider spin-2 dark sector gravitons emission as the DR particles. In this case, we find distinguishable signatures of a non-zero initial PBH spin compared to the pure non-spinning case.

The paper is organized as follows: in section 2, we estimate the effects of including initial PBH spins compared to the non-spinning case in the background evolution, and in section 3, the corresponding impacts in ISGWB are discussed. We use section 4 to study the possibilities of dark radiation, dark matter, and baryogenesis for particles emitted from initially spinning PBHs. Finally, we discuss our results and implications in section 5. We work with $c = \hbar = k_B = 1$ and also set the reduced Planck mass $M_{\text{Pl}}^2 = (8\pi G)^{-1}$ to unity, unless explicitly written.

2 Spinning PBHs, their evaporation, and the background evolution

It is well known that black holes (BH) evaporate via Hawking radiation, and the emitted particles exhibit a near thermal spectrum. For the case of a Schwarzschild (non-rotating and uncharged) BH, the horizon temperature is given by

$$T_{\text{PBH}}^{\text{S}} = \frac{M_{\text{Pl}}^2}{M_{\text{PBH}}} \simeq 1.053 \text{ GeV} \left(\frac{10^{13} \text{ g}}{M_{\text{PBH}}} \right), \quad (2.1)$$

and the lifetime of a BH or the time scale of its complete evaporation can be written as,

$$\Delta t_{\text{PBH}}^{\text{S}} \approx \frac{160 M_{\text{PBH}}^3}{\pi \mathcal{G} \overline{g_{*,H}} M_{\text{Pl}}^4}. \quad (2.2)$$

Here the graybody factor $\mathcal{G} \approx 3.8$, $g_{*,H}$ is the number of degrees-of-freedom for particles with masses below T_{BH} and $\overline{g_{*,H}}$ is average over PBH lifetime [76, 114]. These formulas get modified for spinning PBHs. For a spinning (but uncharged) PBH, the horizon temperature is given by,

$$T_{\text{PBH}} = \frac{M_{\text{Pl}}^2}{M_{\text{PBH}}} \left(\frac{2\sqrt{1-a_*^2}}{1 + \sqrt{1-a_*^2}} \right), \quad (2.3)$$

where a_* is the reduced spin parameter, defined by $a_* = JM_{\text{Pl}}^2/M_{\text{PBH}}^2$ and J is the magnitude of the angular momentum. The time evolution of mass and spin follow the first-order coupled differential equations,

$$\frac{dM(t)}{dt} = -\varepsilon(M(t), a(t)) \frac{M_{\text{Pl}}^4}{M(t)^2}, \quad (2.4)$$

$$\frac{da(t)}{dt} = -a(t) \left[\gamma(M(t), a(t)) - 2\varepsilon(M(t), a(t)) \right] \frac{M_{\text{Pl}}^4}{M(t)^3}. \quad (2.5)$$

Here γ and ε are to be determined by taking into account the sum of contributions from all possible stable and unstable particles emitted due to the Hawking radiation and are functions of PBH mass $M(t)$ and spin $a(t)$ at time t [114–118]. For spinning PBHs, evaporation is more efficient, and the rate increases. We solve equation (2.4) and (2.5) to obtain the lifetime of a spinning PBH, Δt_{PBH} , which depends both on the initial spin and mass of PBH and

a_*	$M_{\text{PBH}} = 10^2 \text{ g}$	$M_{\text{PBH}} = 10^4 \text{ g}$	$M_{\text{PBH}} = 10^6 \text{ g}$	$M_{\text{PBH}} = 10^8 \text{ g}$
0.0	1.0	1.0	1.0	1.0
0.1	0.976899	0.967814	0.972579	0.975514
0.2	0.962462	0.951945	0.957989	0.961175
0.3	0.938191	0.928076	0.930649	0.936888
0.4	0.903097	0.894256	0.896733	0.901647
0.5	0.858785	0.849704	0.852926	0.857398
0.6	0.804028	0.79565	0.798765	0.802748
0.7	0.736373	0.728771	0.731148	0.735063
0.8	0.654221	0.64797	0.650297	0.652996
0.9	0.555112	0.549758	0.55136	0.553933
0.99	0.439075	0.435225	0.437123	0.438618
0.999	0.421827	0.417918	0.419717	0.421357

Table (1) We tabulate the values of the function $\mathcal{F}(a_*, M_{\text{PBH}})$ for spinning PBHs for different values of a_* and for four reference values of M_{PBH} , computed using the code **BlackHawk**. We find that the dependence of $\mathcal{F}(a_*, M_{\text{PBH}})$ on the PBH mass is weak and thus can be neglected for the PBHs mass range of our interest.

introduce $\mathcal{F}(a_*, M_{\text{PBH}})$ as the ratio between Δt_{PBH} and the lifetime of the Schwarzschild PBH as, $\Delta t_{\text{PBH}}^{\text{S}}$,

$$\Delta t_{\text{PBH}} = \Delta t_{\text{PBH}}^{\text{S}} \mathcal{F}(a_*, M_{\text{PBH}}). \quad (2.6)$$

Since the function $\mathcal{F}(a_*, M_{\text{PBH}})$ can not be calculated analytically, we estimate it numerically using the publicly available code **BlackHawk** [119, 120]. We have tabulated the values of $\mathcal{F}(a_*, M_{\text{PBH}})$ computed using **BlackHawk**¹ in Table 1. As evident from this table, for the mass range of our interest, $\mathcal{F}(a_*, M_{\text{PBH}})$ bears a negligible dependence on M_{PBH} , and we can write,

$$\Delta t_{\text{PBH}} \approx \Delta t_{\text{PBH}}^{\text{S}} \mathcal{F}(a_*). \quad (2.7)$$

This allows us to fit the function with a polynomial of a_* as

$$\mathcal{F}(a_*) = \sum_{n=0}^4 c_n a_*^n + \mathcal{O}(a_*^5), \quad (2.8)$$

where we neglect the higher-order terms as their contribution becomes insignificant. We find the values of coefficients c_n as; $c_0 = 1.0, c_1 = -0.183014, c_2 = -0.086326, c_3 = -0.195741$ and $c_4 = -0.110894$ to fit the numerically obtained $\mathcal{F}(a_*)$. The very weak dependence of $\mathcal{F}(a_*)$ on initial mass M_{PBH} is evident from the right panel of figure 1 as the data points for different M_{PBH} fall on top of each other. The left panel of Fig. 1 shows the time evolution

¹We find a slight mismatch between the values of $\mathcal{F}(a_*, M_{\text{PBH}})$ from **BlackHawk** and **FRISBHEE** [118]. For the estimation of $\mathcal{F}(a_*, M_{\text{PBH}})$ and interpolation in equation (2.8), we only use the results from **BlackHawk**.

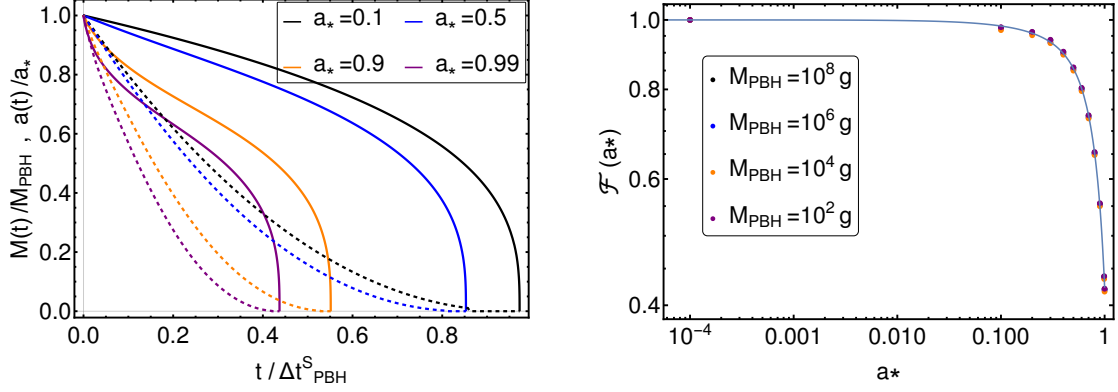


Figure (1) **Left panel:** The evolution of the ratio of PBHs mass $M(t)$ to their initial mass M_{PBH} (solid lines) and the ratio of spin parameter $a(t)$ to its initial value a_* (dashed lines) as a function of time. We normalize the time axis by dividing it by the lifetime of Schwarzschild black hole of the same mass, Δt_{PBH}^S . We take four different initial values of a_* with initial PBH mass $M_{\text{PBH}} = 10^6$ g. **Right panel:** We plot $\mathcal{F}(a_*)$ as a function of initial value of PBH spin parameter a_* for four different initial PBH masses. The data points correspond to the numerical result from **BlackHawk** while the continuous line represents a polynomial interpolation of $\mathcal{F}(a_*)$ which nicely fits the $\mathcal{F}(a_*, M_{\text{PBH}})$ values obtained from the full numerical calculation.

of mass and spin of the BHs. It is clear that spin and mass evolve very differently during Hawking evaporation. While mass changes very rapidly near the end of the evaporation process, the spin depletes much earlier. As we go towards higher initial values of a_* , the lifetimes decrease more compared to Schwarzschild lifetime.

In our setup, we consider the ultra-low mass PBHs to form during early radiation-dominated epoch after inflation (at conformal time $\tau = \tau_f$) with initial abundance β_f . We assume that this population of PBHs dominates the universe at $\tau = \tau_m$, which lasts until their evaporation at $\tau = \tau_r$. Since we are mainly interested in calculating the resonant second-order ISGWB contribution, [108], the PBH domination and almost instantaneous transition from matter domination to the standard radiation domination (RD) due to the Hawking evaporation play a very important role in the amplification of the ISGWB generated at the onset of RD [80]. Using the results of our previous work [80], we can calculate the conformal times associated with the PBH evaporation τ_r as,

$$\tau_r = \sqrt{2} \left(\frac{3\Delta t_{\text{PBH}}^2 \rho_{\text{EQ}} \tau_{\text{EQ}}^4}{M_{\text{Pl}}^2} \right)^{1/4} \quad (2.9)$$

and the ratio τ_{rat} between the conformal times of PBH evaporation (τ_r) and PBH domination (τ_m),

$$\tau_{\text{rat}} \equiv \frac{\tau_r}{\tau_m} = 2 \left(\frac{3\pi^2 M_{\text{Pl}}^6 \beta_f^4 \tau_r^4}{M_{\text{PBH}}^2 \rho_{\text{EQ}} \tau_{\text{EQ}}^4} \right)^{1/6}. \quad (2.10)$$

Here the subscript "EQ" refers to various quantities evaluated at the standard radiation-matter equality. As evident from eqs. (2.9) and (2.10), initial non-zero values of a_* modify the

lifetime of the PBHs Δt_{PBH} , and thereby affect the time duration for both PBHs domination and their evaporation. To stay within the validity of linear perturbation theory for first order scalar modes, we need to stay in the regime where $\tau_{\text{rat}} \leq 470$ [101, 108, 121]. We shall refer to this limit as non-linearity bound for the rest of our paper.

For each conformal time τ_Y , we get a comoving wavenumber $k_Y \equiv 1/\tau_Y$, which re-enters the horizon at $\tau = \tau_Y$. It is also possible to express the values of these relevant wavenumbers in terms of $\mathcal{F}(a_*)$. Taking $k_{\text{EQ}} = 1/\tau_{\text{EQ}} \simeq 0.01 \text{ Mpc}^{-1}$ and $H_{\text{EQ}} \simeq 20.7 \text{ Mpc}^{-1}$, we get

$$k_r = \frac{1}{\tau_r} \approx 2.1 \times 10^{11} [\mathcal{F}(a_*)]^{-1/2} \left(\frac{M_{\text{PBH}}}{10^4 g} \right)^{-3/2} \text{Mpc}^{-1}, \quad (2.11)$$

$$k_m = \frac{\tau_{\text{rat}}}{\tau_r} \approx 3.4 \times 10^{17} [\mathcal{F}(a_*)]^{-1/6} \left(\frac{M_{\text{PBH}}}{10^4 g} \right)^{-5/6} \beta_f^{2/3} \text{Mpc}^{-1}, \quad (2.12)$$

$$k_f = \frac{k_m}{\beta_f} \approx 3.4 \times 10^{17} [\mathcal{F}(a_*)]^{-1/6} \left(\frac{M_{\text{PBH}}}{10^4 g} \right)^{-5/6} \beta_f^{-1/3} \text{Mpc}^{-1}. \quad (2.13)$$

Note that the comoving scale k_r does not depend on β_f while both k_m and k_f explicitly depend on it. All these scales also depend upon $\mathcal{F}(a_*)$ and play a crucial role in our later analysis. Since all the PBHs will be evaporated by the time τ_r , the comoving wavenumber k_r is associated with the transition from early matter-dominated (eMD) to the standard RD and also indicates the time of the ISGWB generation. The scale k_m points to the cutoff scale in the inflationary scalar perturbation spectrum, which leads to the first resonant peak in the ISGWB. Finally, the scale of PBH formation k_f is directly related to the mass of PBHs and plays an important role in determining the cutoff scale for the PBH-induced isocurvature perturbations and, thus, the second peak of the ISGWB.

3 Induced stochastic gravitational wave background (ISGWB) from spinning PBHs

As we discussed in the previous section, evaporating PBHs with spin have slightly different lifetimes than the non-spinning ones. Since we focus on a scenario wherein the PBH evaporation initiates the standard RD epoch, this shift in the PBH lifetime also induces a shift in the start of the standard RD, as well as all the other relevant time scales, such as the start of PBH domination, PBH formation, etc., as shown in eqns. (2.11), (2.12) and (2.13).

In our previous work [80], we estimated the resonant ISGWB from two different components of adiabatic scalar perturbations; the inflationary adiabatic and the isocurvature-induced adiabatic component. In these scenarios, the source of isocurvature perturbations is the formation of PBHs, which converts to adiabatic perturbations by the time PBHs dominate the universe. The cutoff scale of the initial isocurvature power spectrum, k_{UV} , is taken at the scale of the mean distance between two black holes at their formation to avoid the granularity of the PBH fluid [112]. Taking the efficiency factor associated with PBH formation in early RD, $\gamma \approx 0.2$ we can write,

$$k_{\text{UV}} = \left(\frac{\beta_f}{\gamma} \right)^{1/3} k_f. \quad (3.1)$$

The analytical expressions derived in our previous paper [80] makes it easy to infer that the ISGWB spectrum, in this case, explicitly depends on the three wavenumbers associated with

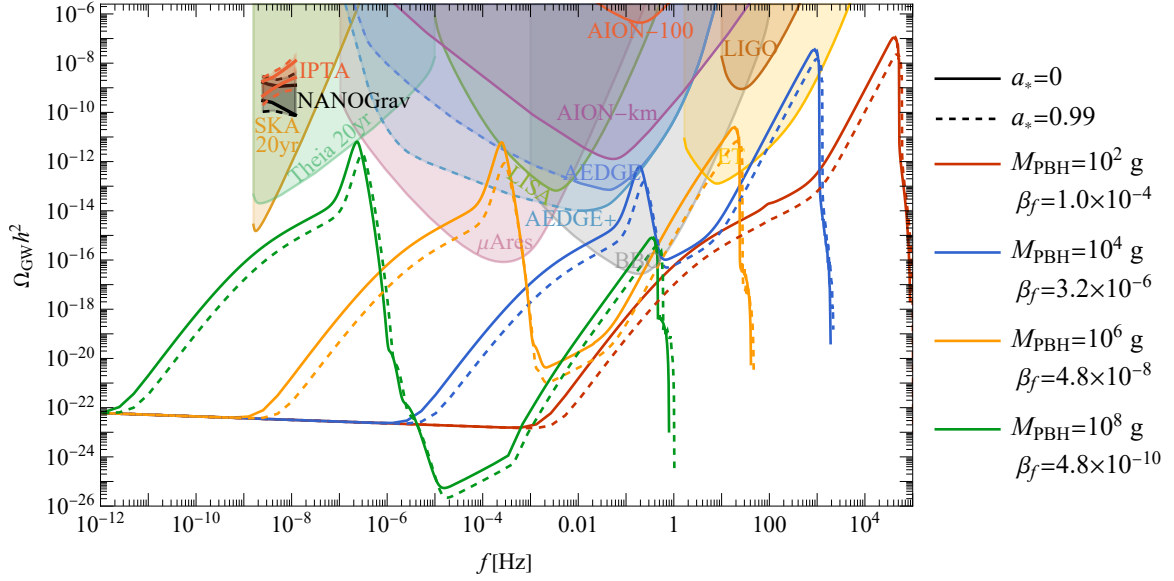


Figure (2) The spectral energy density $\Omega_{\text{GW}} h^2$ of the ISGWB for selected representative populations of spinning and non-spinning PBHs with monochromatic mass range. These populations are characterized by two parameters: β_f , the initial mass fraction of PBHs at their formation, and M_{PBH} , the initial PBH mass. The solid and dashed lines show our results for ISGWB for PBH populations with no spin ($a_* = 0$) and with spin ($a_* = 0.99$), respectively. For all these cases, the doubly peaked profiles of ISGWB correspond to the secondary contribution sourced by the inflationary adiabatic and the isocurvature induced adiabatic scalar perturbations, respectively.

the PBH formation, domination, and evaporation; k_f , k_m , k_r and the initial PBH abundance β_f . The modifications in the ISGWB due to the change in the initial PBH spin arise only through the spin dependence of these wavenumbers, as we derived in the previous section. The final form of the ISGWB spectrum today, from isocurvature contribution [80],

$$\Omega_{\text{GW}}(\tau_0, k) = c_g \Omega_{r,0} \mathcal{J} \int_{-s_0}^{s_0} \frac{27 \sqrt[3]{3} (s^2 - 1)^2}{(9 - 3s^2)^{5/3}} ds \quad (3.2)$$

where $c_g \approx 0.4$ if we take the number of relativistic degrees of freedom to be ~ 106.7 , $\Omega_{r,0}$ is the present radiation energy density. The limit of s integral s_0 is defined as a function of k ;

$$s_0 = \begin{cases} 1 & \frac{k}{k_{\text{UV}}} \leq \frac{2}{1+\sqrt{3}} \\ 2 \frac{k_{\text{UV}}}{k} - \sqrt{3} & \frac{2}{1+\sqrt{3}} \leq \frac{k}{k_{\text{UV}}} \leq \frac{2}{\sqrt{3}} \end{cases} \quad (3.3)$$

and we can write,

$$\mathcal{J} \approx 2.0 \times 10^{-12} \beta_f^{16/3} \left(\frac{f}{1 \text{ Hz}} \right)^{11/3} \left(\frac{M_{\text{PBH}}}{1 \text{ g}} \right)^{41/6} \mathcal{F}(a_*)^{5/2},$$

$$\frac{k}{k_{\text{UV}}} \approx 4.8 \times 10^{-7} \left(\frac{M_{\text{PBH}}}{1 \text{ g}} \right)^{5/6} \mathcal{F}(a_*)^{1/6} \left(\frac{f}{1 \text{ Hz}} \right),$$

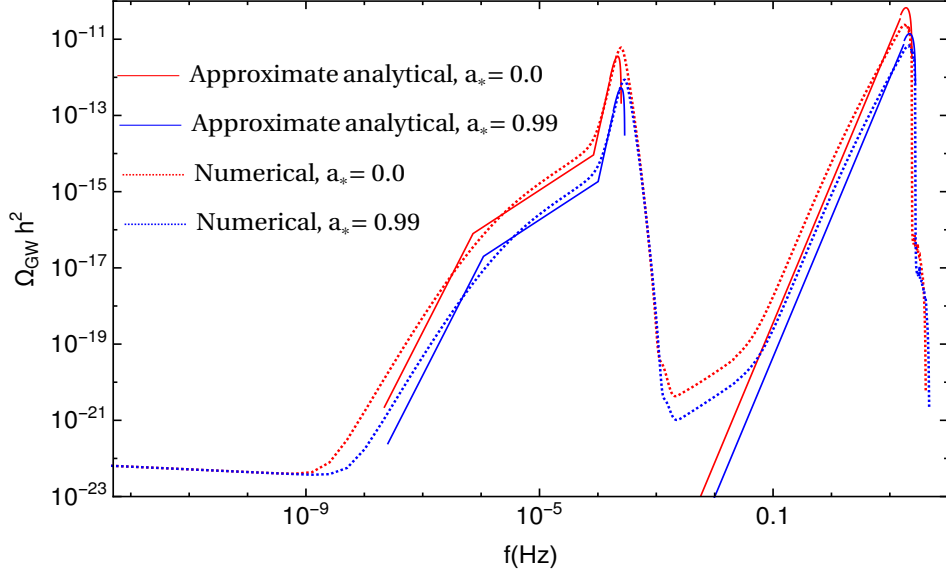


Figure (3) We compare the analytical (solid lines) and numerical (dotted lines) results for ISGWB spectral energy density $\Omega_{\text{GW}} h^2$ for initial PBH mass $M_{\text{PBH}} = 10^6 g$ and $\beta_f = 4.5 \times 10^{-8}$ for spinning ($a_* = 0.99$) and non-spinning ($a_* = 0.0$) population of PBHs. While the dotted lines are from an exact numerical calculation, the solid lines are due to the approximate analytical expressions we derived in equations (3.2) and (3.6).

in terms of the mass of the PBHs M_{PBH} , initial abundance β_f and spin parameter a_* , after taking the shift in PBH lifetime for spinning PBHs correctly into account. This leads to a peak value for the second ISGWB peak,

$$\Omega_{\text{GW}}(\tau_0) \Big|_{k=k_{\text{UV}}} \approx 1.9 \times 10^6 \beta_f^{16/3} \left(\frac{M_{\text{PBH}}}{1g} \right)^{34/9} \mathcal{F}(a_*)^{17/9} \quad (3.4)$$

The first or the low-frequency peak of the ISGWB spectrum corresponds to the resonant contribution from inflationary adiabatic perturbations. We consider the standard power-law power spectra for inflationary scalar curvature perturbations,

$$\mathcal{P}_{\mathcal{R}} = A_s \left(\frac{k}{k_p} \right)^{n_s - 1}, \quad (3.5)$$

with pivot scale $k_p = 0.05 \text{ Mpc}^{-1}$, scalar amplitude $A_s = 2.09 \times 10^{-9}$ and scalar index $n_s = 0.965$ [122], which leads to the first peak of ISGWB [80, 108],

$$\frac{\Omega_{\text{GW}}(\tau_0, k)}{A_s^2 c_g \Omega_{r,0}} \simeq \begin{cases} 3 \times 10^{-7} x_r^3 x_{\text{max}}^5 & 150 x_{\text{max}}^{-5/3} \lesssim x_r \ll 1 \\ 6.6 \times 10^{-7} x_r x_{\text{max}}^5 & 1 \ll x_r \lesssim x_{\text{max}}^{5/6} \\ 3 \times 10^{-7} x_r^7 & x_{\text{max}}^{5/6} \lesssim x_r \lesssim \frac{2}{1+\sqrt{3}} x_{\text{max}} \\ \mathcal{C}(k) & \frac{2}{1+\sqrt{3}} \leq \frac{x_r}{x_{\text{max}}} \leq \frac{2}{\sqrt{3}} \end{cases}, \quad (3.6)$$

where

$$\mathcal{C}(k) = 0.00638 \times 2^{-2n_s-13} 3^{n_s} x_r^7 s_0 \left(\frac{x_r}{x_{\max}} \right)^{2n_s-2} \times \left[-s_0^2 {}_2F_1 \left(\frac{3}{2}, -n_s; \frac{5}{2}; \frac{s_0^2}{3} \right) + 4 {}_2F_1 \left(\frac{1}{2}, 1-n_s; \frac{3}{2}; \frac{s_0^2}{3} \right) - 3 {}_2F_1 \left(\frac{1}{2}, -n_s; \frac{3}{2}; \frac{s_0^2}{3} \right) \right]. \quad (3.7)$$

and,

$$\begin{aligned} x_r &= k/k_r \approx 0.001 \left(\frac{f}{1 \text{ Hz}} \right) \left(\frac{M_{\text{PBH}}}{1g} \right)^{3/2} \sqrt{\mathcal{F}(a_*)}, \\ x_{\max} &= k_m/k_r \approx 2.36 * 10^3 \beta_f^{2/3} \left(\frac{M_{\text{PBH}}}{1g} \right)^{2/3} \mathcal{F}(a_*)^{1/3}, \\ s_0 &= 2 \frac{k_m}{k} - \sqrt{3} \approx 1.16 * 10^{-6} \left(\frac{f}{1 \text{ Hz}} \right) \beta_f^{-2/3} \left(\frac{M_{\text{PBH}}}{1g} \right)^{5/6} \mathcal{F}(a_*)^{1/3} - \sqrt{3}. \end{aligned}$$

The peak of the inflationary adiabatic contribution for ISGWB is expected to appear at $k = k_m$, and turns out to be,

$$\Omega_{\text{GW}}(\tau_0) \Big|_{k=k_m} \approx 6.9 \times 10^{-6} \beta_f^{14/3} \left(\frac{M_{\text{PBH}}}{1g} \right)^{14/3} \mathcal{F}(a_*)^{7/3} \quad (3.8)$$

$$\approx 1.7 \times 10^{-29} \left(\frac{k_m}{k_r} \right)^7 \equiv 1.7 \times 10^{-29} \left(\frac{\tau_r}{\tau_m} \right)^7. \quad (3.9)$$

To stay within the validity of linear perturbation theory for scalar modes, we restrict our study only in the regime where $\left(\frac{\tau_r}{\tau_m} \right) \leq 470$ [101, 108, 121], which puts a strict bound on the inflationary adiabatic peak,

$$\Omega_{\text{GW}}(\tau_0) \Big|_{k=k_m} \leq 8.4 \times 10^{-11}. \quad (3.10)$$

To check the viability of analytical results of equation (3.2) and (3.6), we plot it along with numerically obtained ISGWB spectral energy density $\Omega_{\text{GW}} h^2$ in Fig. 3 both for spinning and non-spinning PBHs. As we discussed in section 2, we use $\mathcal{F}(a_*, M_{\text{PBH}})$, obtained from **BlackHawk** to numerically compute the ISGWB spectrum for spinning PBHs. In Fig. 2, we plot the ISGWB spectra for PBH mass range $10^2 - 10^8$ g with appropriate mass fractions, both for initially spinning and non-spinning PBHs, along with the projected sensitivities [123] of LIGO [124, 125], SKA [126], LISA [127, 128], AEDGE [129, 130], AION/MAGIS [129, 131–133], ET [134, 135], BBO [136, 137], μARES [138], and Theia[139]. We also show fits to the possible signal reported by PTA collaborations [140–143]. Both from Figs. 2 and 3, weak dependence of ISGWB on the initial PBH spin is quite evident.

In this work, we are primarily interested in the domination and evaporation signatures of ultra-light PBHs and we remain agnostic about their generation mechanism. As the simplest possible case, we take both the initial mass and spin distributions to be monochromatic. However, a broader distribution for PBH spin and mass can be more attractive in the context of a specific PBH formation mechanism. For broader distribution of either PBH mass or spin would lead to a longer duration of the transition from PBH domination to RD phase and, therefore, will suppress the resonant ISGWB peaks for both isocurvature-induced and inflationary adiabatic peaks. As the suppression effects are more dominant for higher wavenumber

modes [109], we can expect that the isocurvature peak will be more strongly affected than the inflationary one. Recently, effects of broader PBH mass distributions have been studied in the context of isocurvature-induced ISGWB peak [113]. Since an accurate estimation of the ISGWB for a broader spin or mass distribution requires an integrated setup to carefully keep track of the adiabatic and isocurvature scalar modes and second-order tensor modes during the transition, we leave this analysis for future work.

4 Signatures of spinning PBHs in different scenarios

The Hawking evaporation of PBHs takes place via the emission of all kinds of particles depending on the properties of the emitted particles and the mass and angular momentum of the evaporating PBH. In this process, the mass and angular momentum of a PBH is dissipated, which depends on its initial properties. The rate of emission for a particular particle species i , with spin s_i in the energy interval $(E, E + dE)$ can be expressed as [69, 119, 120],

$$\frac{d^2 N_i}{dt dE} = \frac{g_i}{2\pi} \sum_{\ell, m} \Gamma_{s_i \ell m} [E, M_{\text{BH}}(t), a_*(t)] \frac{1}{e^{(E_i - m\Omega)/T_{\text{BH}}(t)} - (-1)^{2s_i}}, \quad (4.1)$$

with the total energy $E^2 = p^2 c^2 + m_i^2 c^4$, particle mass m_i , and projection to the angular momentum $m \in [-\ell, +\ell]$, $\Omega = (4\pi/M_{\text{BH}})(a_*/(1 + \sqrt{1 - a_*^2}))$ is the angular velocity of the horizon and internal degrees of freedom (DOF) g_i accounts for the polarization and color DOF. The graybody factors $\Gamma_{s_i \ell m}$ characterize the probabilities for the emitted species not to be re-absorbed, escaping the gravitational well of the BH, which are a function of E , $M_{\text{BH}}(t)$, $a_*(t)$, g_i , s_i and m_i .

Different particles emitted from the PBHs can contribute to very different physical phenomena. Massive non-relativistic particles emitted from PBHs can contribute to the observed matter anti-matter asymmetry in our universe through their baryon number violating decay, which we considered in our previous work [80]. On the other hand, Hawking-production of massive non-relativistic stable dark-sector particles can account for our universe's total dark matter budget while the production of dark sector light relativistic particles can contribute to the dark radiation [66].

4.1 Dark radiation

The relativistic dark sector particles emitted from Hawking radiation of PBHs would add to the total radiation energy density. Since the background dynamics are probed very precisely both during CMB and BBN eras, this extra dark radiation (DR) component can be constrained. Although the effects of a broader spin distribution in the context of DR have been studied earlier [70], similar to the previous section, we restrict our analysis to the case of a monochromatic mass and spin distribution of PBHs, while estimating the DR contribution in this section.

We usually parameterize the presence of this extra radiation in terms of the effective number of relativistic degrees of freedom, ΔN_{eff} . The total radiation energy density can be written as a sum of the bosonic and fermionic components,

$$\rho_{\text{rad}} = \frac{\pi^2}{30} \left[\sum_b g_{*b} \left(\frac{T_b}{T} \right)^4 + \frac{7}{8} \sum_f g_{*f} \left(\frac{T_f}{T} \right)^4 \right] T^4. \quad (4.2)$$

After neutrino decoupling, when the temperature drops below the electron mass, electron-positron annihilates together to produce photons. Thus the entropy of the electrons and positrons is transferred to the photons but not to the decoupled neutrinos. This leads to a relative difference between photon and neutrino temperatures,

$$T_\nu = (4/11)^{1/3} T_\gamma, \quad (4.3)$$

and using (4.2) we have,

$$\rho_R = \rho_\gamma \left[1 + \frac{7}{8} \left(\frac{4}{11} \right)^{4/3} N_{\text{eff}} \right]. \quad (4.4)$$

In the presence of an additional dark radiation component from PBHs evaporation, we can express it with,

$$\rho_R + \rho_{\text{DR}} = \rho_\gamma \left[1 + \frac{7}{8} \left(\frac{4}{11} \right)^{4/3} (N_{\text{eff}}^{\text{SM}} + \Delta N_{\text{eff}}) \right]. \quad (4.5)$$

At matter-radiation equality ($\tau = \tau_{\text{EQ}}$), we can therefore, write ΔN_{eff} as

$$\Delta N_{\text{eff}} \Big|_{\text{DR}} = \left\{ \frac{8}{7} \left(\frac{4}{11} \right)^{-\frac{4}{3}} + N_{\text{eff}}^{\text{SM}} \right\} \frac{\rho_{\text{DR}}(\tau_{\text{EQ}})}{\rho_R(\tau_{\text{EQ}})}, \quad (4.6)$$

and it is straightforward to connect it with the quantities at the time of PBH evaporation ($\tau = \tau_r$),

$$\frac{\rho_{\text{DR}}(\tau_{\text{EQ}})}{\rho_R(\tau_{\text{EQ}})} = \frac{\rho_{\text{DR}}(\tau_r)}{\rho_R^{\text{SM}}(\tau_r)} \left(\frac{g_*(T_r)}{g_*(T_{\text{EQ}})} \right) \left(\frac{g_{*S}(T_{\text{EQ}})}{g_{*S}(T_r)} \right)^{\frac{4}{3}}. \quad (4.7)$$

While calculating the energy density of dark radiation particles at the time of PBH evaporation $\rho_{\text{DR}}(\tau_r)$, the approximation of instantaneous production of these particles at the very end of PBH evaporation process is quite justified for non-spinning PBHs and for the production of particles with spin ≤ 1 even for spinning PBHs [66, 68, 69, 144]. However, for the spin 2 particles produced from initially spinning PBHs to act as dark radiation particles, this approximation breaks down [118]. The light relativistic particles are produced in the earlier phase of PBH evaporation compared to the massive particles. Thus, by the time the entire PBH evaporates, the initial energy density of these particles dilutes significantly. This effect is more important for PBH domination scenarios because in such a scenario, while the total energy density will dilute as a^{-3} , the energy density of light relativistic particles would dilute as a^{-4} . This effect was pointed out and taken into account by solving the Boltzmann equations for combined fluid composed of SM radiation, dark radiation, and PBH in a publicly available code FRISBHEE [118]. We also use this code for our set-up to calculate $\rho_{\text{DR}}(\tau_r)$ taking into account the redshift effects and to estimate ΔN_{eff} accurately.

As we mentioned, ISGWB also contributes to the radiation energy density and, therefore, to ΔN_{eff} . It is straightforward to generalise equation (4.6) for ISGWB contribution,

$$\Delta N_{\text{eff}} \Big|_{\text{ISGWB}} = \left\{ \frac{8}{7} \left(\frac{4}{11} \right)^{-\frac{4}{3}} + N_{\text{eff}}^{\text{SM}} \right\} \frac{\rho_{\text{GW}}(\tau_{\text{EQ}})}{\rho_R(\tau_{\text{EQ}})} = \left\{ \frac{8}{7} \left(\frac{4}{11} \right)^{-\frac{4}{3}} + N_{\text{eff}}^{\text{SM}} \right\} \frac{\Omega_{\text{GW}}(\tau_0)}{\Omega_R(\tau_0)}. \quad (4.8)$$

The non-linearity bound $\tau_{\text{rat}} \leq 470$ puts a strong constraint on the inflationary adiabatic peak of the ISGWB and this limit in equation (3.10) translates to,

$$\Delta N_{\text{eff}} \Big|_{\text{infl-ISGWB}} \leq 2.5 \times 10^{-5} \quad (4.9)$$

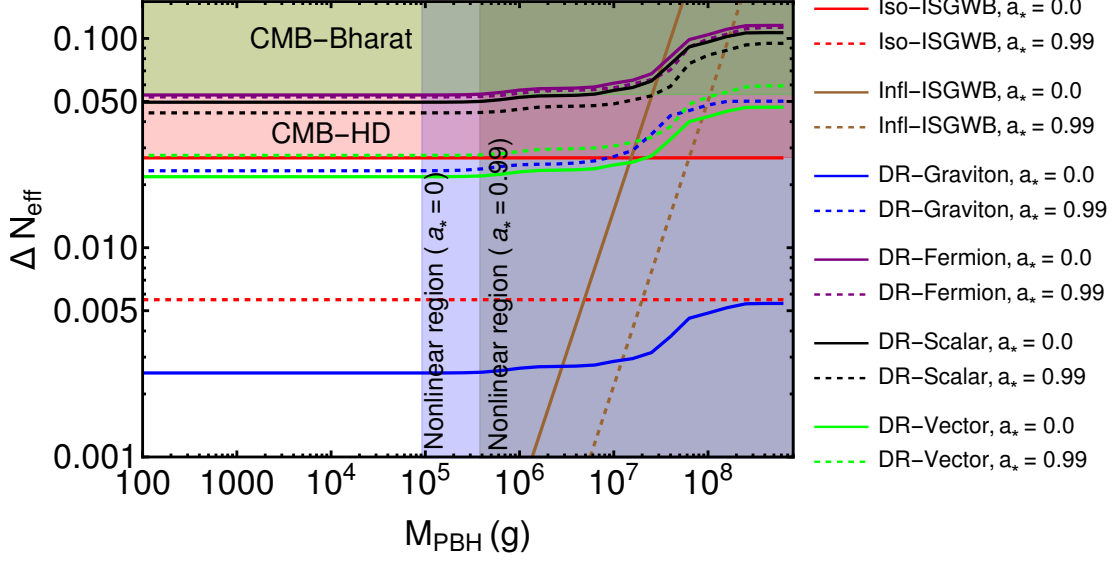


Figure (4) Comparison of different contributions to ΔN_{eff} , while we change the initial abundance of PBHs with changing PBH mass: $\beta_f \propto 1/M_{\text{PBH}}^{17/24}$ to keep ΔN_{eff} contribution from isocurvature induced adiabatic peak of ISGWB (red line) to a constant value and plot corresponding ΔN_{eff} contribution considering different massless dark radiation particles. In these cases, solid lines correspond to $a_* = 0.0$, and dashed lines refer to $a_* = 0.99$. Also, for all these cases, we maintain $\beta_f \left(\frac{M_{\text{PBH}}}{1.0 \text{ g}} \right)^{17/24} = \text{constant}$ and choose this constant appropriately such that the isocurvature induced ISGWB contribution to ΔN_{eff} is comparable. The non-linear regime ($\tau_{\text{rat}} \geq 470$) is shaded in grey, and the CMB-HD and CMB-Bharat sensitivities are displayed with the pink and green shaded regions. We also get detectable ΔN_{eff} from ISGWB peak of inflationary adiabatic perturbation (brown line) only in the non-linear region, as expected from equation (3.9) and (3.10).

which is too small to be probed by BBN or any recent or upcoming CMB observatories. It can also be seen in Fig. 5 and Fig. 4 that ΔN_{eff} from the first peak of ISGWB, is only detectable in the non-linear region and, therefore, is not of our interest.

That only leaves the isocurvature-induced adiabatic contribution of ISGWB to be considered as a candidate for significant contribution to ΔN_{eff} . From (3.4), we can write,

$$\Delta N_{\text{eff}} \Big|_{\text{Iso-ISGWB}} \simeq 5.71 \times 10^{11} \beta_f^{16/3} \left(\frac{M_{\text{PBH}}}{1g} \right)^{34/9} \mathcal{F}(a_*)^{17/9} \quad (4.10)$$

where we take $N_{\text{eff}}^{\text{SM}} \simeq 3.048$ and $\Omega_{\text{R}}(\tau_0)h^2 \simeq 2.5 \times 10^{-5}$ [145]. From equation (4.10), it is evident that the dependence of PBH mass and abundance to ΔN_{eff} comes from $\beta_f^{16/3} M_{\text{PBH}}^{34/9}$ factor for ISGWB contribution. We plot the corresponding DR components keeping this factor to a constant value in Fig. 4. As a result, we obtain the ΔN_{eff} from the isocurvature peak for spinning and non-spinning PBHs, as different constant values. $\mathcal{F}(a_*)$ terms contribute to the difference between spinning and non-spinning PBH cases.

In Fig. 5, we keep the initial PBH abundance β_f fixed and show corresponding ΔN_{eff} contributions for ISGWB and DR. As ISGWB peaks are strongly dependent on M_{PBH} , we

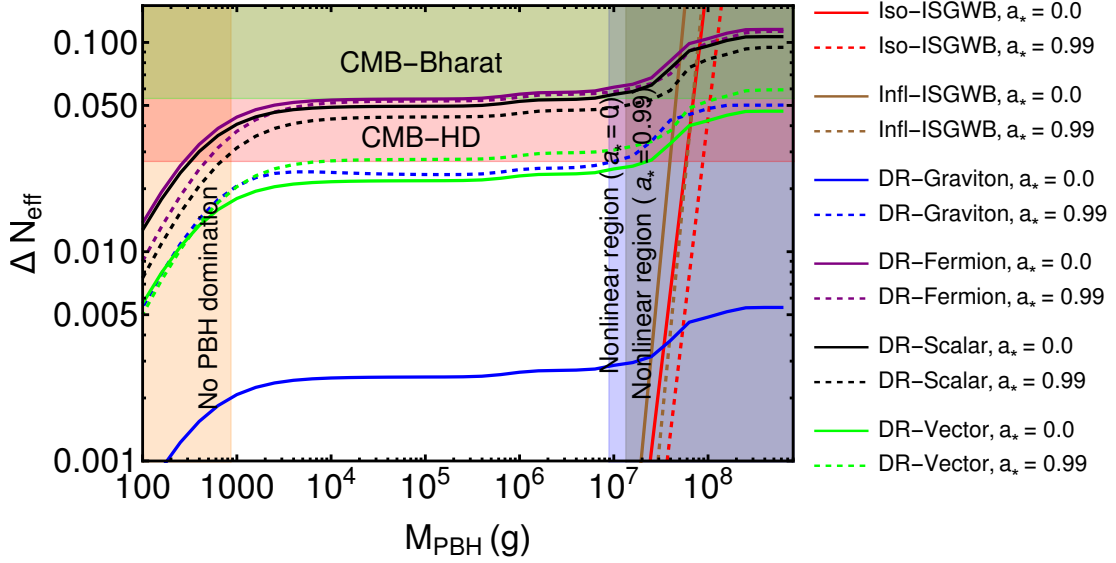


Figure (5) Comparison of different contributions to ΔN_{eff} , while we keep the initial abundance of PBHs fixed $\beta_f = 10^{-8}$ and plot the corresponding ΔN_{eff} contribution from the isocurvature induced adiabatic peak of ISGWB (red line) and different massless DR particles. For each of these cases, solid lines correspond to $a_* = 0.0$, and dashed lines refer to $a_* = 0.99$. The non-linear regime is shaded in grey, the CMB-HD and CMB-Bharat sensitivities with the pink and green shaded regions, and the parameter space of no PBH domination in which they evaporate before they can dominate, in orange. We also plot ΔN_{eff} from an inflationary adiabatic peak of ISGWB (brown line) and find it detectable only in the non-linear region.

get highly tilted lines for ISGWB contributions. The DR contribution reflects a somewhat different nature: for higher mass PBHs, DR contribution is the same as in Fig. 4 and Fig. 5, but for lower mass PBHs, constant β_f results in a suppressed contribution to ΔN_{eff} in Fig. 5, for the region where PBHs evaporate before they can dominate. As we go to even lower mass PBHs, they evaporate earlier, and the fraction of PBHs and the fraction of DR particles emitted from PBHs decreases. This effect leads to suppression in ΔN_{eff} from DR, in the left part of Fig. 5. We can also see from Fig. 4 and Fig. 5 that as long as β_f is large enough to ensure that PBHs dominate the universe before they evaporate, increasing the value of β_f does not lead to a significant difference in ΔN_{eff} .

This difference in nature of ΔN_{eff} from ISGWB and DR suggests a novel complementarity. While ΔN_{eff} from DR is not very sensitive to either the initial abundance of PBHs β_f or PBH mass M_{PBH} and can only differentiate whether there was a PBH domination epoch or not, ΔN_{eff} from ISGWB has a razor-sharp sensitivity with changing values of β_f and M_{PBH} . For the DR contributions, we consider massless particles with spin $s = 0, 1/2, 1$ and 2. As the PBH spin increases, the distribution of emitted particles favors higher spin particles. We can see this trend from Fig. 4 and 5. For the scalar or $s = 0$ particles, spinning PBHs contribute less to ΔN_{eff} than the Schwarzschild case, but as we go towards higher spin particles, the contribution from spinning PBH increases. For fermions with $s = 1/2$, spinning and non-spinning PBHs contribute almost equally; for $s = 1$ vector particles, spinning PBHs

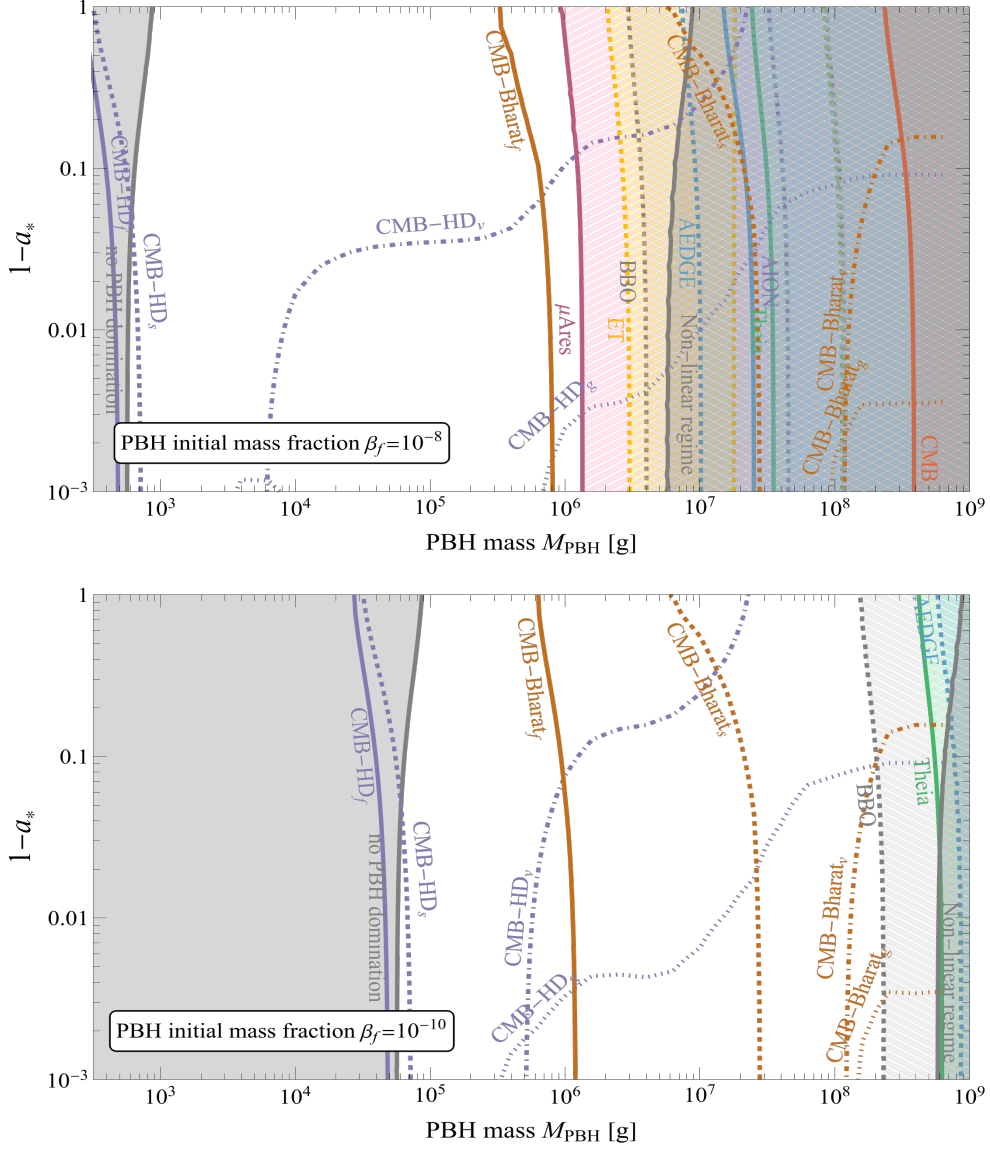


Figure (6) The various contours display the reach of the indicated GW observatories and future CMB experiments due to the produced DR for two different choices of the PBH initial mass fraction β_f . The detection of each of our two peaks is indicated in a separate way for each experiment: low-frequency inflationary adiabatic contribution detection is shown by ‘/’ dashed filling and solid contours, while the high-frequency isocurvature-induced adiabatic peak is indicated by ‘\’ dashed filling and dashed contours. We assume one extra scalar, fermionic, vector, or graviton particle indicated by the subscripts s, f, v , or g to be responsible for DR production. For the lines denoted by CMB-HD or CMB-Bharat, the higher M_{PBH} and smaller $1 - a_*$ region denotes the parameter-space where ΔN_{eff} from DR is detectable in these experiments. The grey region on the left corresponds to the ‘No PBH domination’ while the grey region on the right indicates the ‘Non-linear regime’.

contribute slightly more than non-spinning ones, but this difference becomes visibly large for $s = 2$ graviton particles. For gravitons, the spinning PBHs produce an order of magnitude higher value of ΔN_{eff} compared to the Schwarzschild case.

It is evident from Figs. 4 and 5, that while the scalar and fermion contributions to ΔN_{eff} are relevant for the projected sensitivities of both CMB-HD [146] and CMB-Bharat [147] experiments, the graviton, and vector contributions can only be probed by CMB-HD experiment. We do not show the sensitivity of any other future CMB experiments like CMB-S4 [148] as they are not sensitive to our expected ΔN_{eff} contribution from DR. As the graviton contribution shows a strong dependence on the initial PBH spin, we can obtain a PBH mass dependent critical value for a_* , only above which we can expect associated ΔN_{eff} to be detectable in CMB-HD experiment.

In Fig. 6, we show the effects of changing PBH spin in a more detailed manner and connect detection sensitivities for different GW detectors with existing and projected CMB observational bounds on ΔN_{eff} both for DR and ISGWB contributions. Similar to our earlier work [80], we set the detection criteria in terms of signal-to-noise ratio (SNR),

$$\text{SNR} \equiv \sqrt{\mathcal{T} \int df \left[\frac{\Omega_{\text{GW}}(f)}{\Omega_{\text{noise}}(f)} \right]^2} \geq 10. \quad (4.11)$$

Assuming the operation time $\mathcal{T} = 4$ yr for each experiment, we calculate the SNR by using the noise curve of a given experiment and display the results for the entire parameter space of interest in figure 6. We also show (the solid red line in Fig. 6) the strong upper bound on the parameter space coming from the overproduction of GWs spoiling the CMB [149, 150].

4.2 Dark matter relic density

PBH evaporation can lead to the non-thermal production of stable heavy DM particles. We can also consider light mass DM particles from Hawking evaporation, but as they are highly constrained from particle physics experiments, instead, we focus on heavier mass DM particles in the form of Dirac fermions. Our approach to estimating the present-day DM relic density has been twofold. We use a numerical setup for exact estimates and compare it with independently derived approximate analytical results.

To take into account the continuous production of DM particles from Hawking evaporation and simultaneously the dilution effects from the expansion of the universe, we implement FRISBHEE, which solves Friedmann's equations to estimate the DM energy density at the start of standard RD epoch, primarily contributed at the very last stage of PBH evaporation, when the universe goes through a transition from PBH domination to standard RD. The present-day DM energy density is then obtained using the ratio between then and present-day temperature and the change in the total number of relativistic degrees of freedom. From the conservation of entropy, we can write,

$$a(t_1)^3 g_{*,S}(T_1) T_1^3 = a(t_2)^3 g_{*,S}(T_2) T_2^3 \implies \left(\frac{a(t_1)}{a(t_2)} \right) = \left(\frac{T_2}{T_1} \right) \left(\frac{g_{*,S}(T_2)}{g_{*,S}(T_1)} \right)^{1/3}. \quad (4.12)$$

Using this, the DM energy density $\rho_{\text{DM}}(t_r)$ of the start of RD ($t = t_r$) can be translated to present day ($t = t_0$) DM energy density $\rho_{\text{DM}}(t_0)$ as,

$$\left(\frac{\rho_{\text{DM}}(t_0)}{\rho_{\text{DM}}(t_r)} \right) = \left(\frac{a(t_r)}{a(t_0)} \right) = \left(\frac{T_0}{T_r} \right)^3 \left(\frac{g_*(T_0)}{g_*(T_r)} \right). \quad (4.13)$$

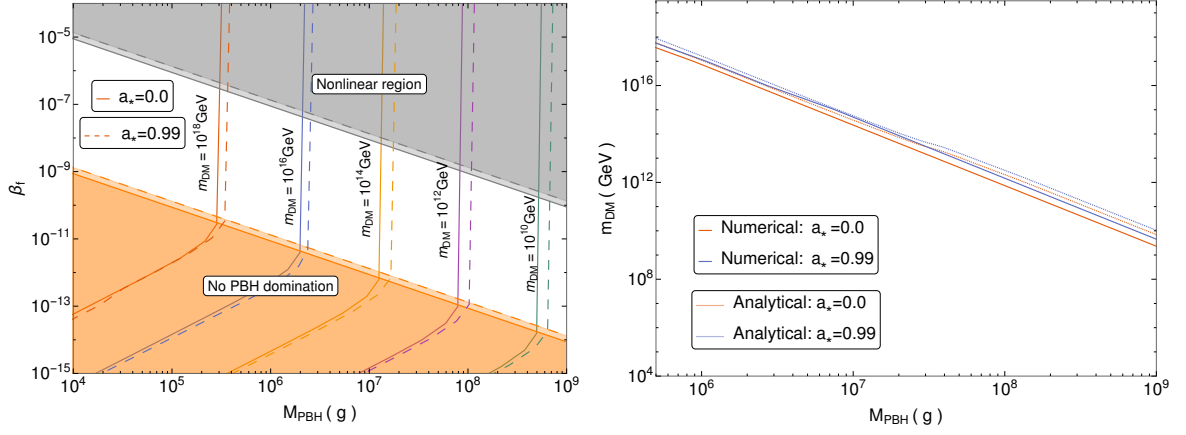


Figure (7) **Left panel:** We plot the values of the initial PBH abundance, β_f as a function of PBH mass for the different masses of the DM particles, which contributes to the observed DM density of our universe ($\Omega_{\text{DM}} h^2 \approx 0.12$ [145]). The non-linear regime ($\tau_{\text{rat}} \geq 470$) is shaded in grey, and no PBH domination region is in orange. **Right panel:** We set β_f such that we get an era of PBH domination and plot the mass of the heavy DM particles, satisfying the observational DM relic density. We also find good agreement between the analytical result for m_{DM} (as in eqn. 4.21) and exact numerical calculation.

We numerically scan the PBH parameter space, namely the PBH mass and initial abundance considering the different mass of DM particles m_{DM} which can produce the observed DM abundance $\Omega_{\text{DM}} h^2 \approx 0.12$ [145], for two different initial spin values $a_* = \{0.0, 0.99\}$, as shown in the left panel of Fig. 7.

We find that the change in the initial spin leaves a small but nonzero shift in the contours, which connects the points in PBH parameter space corresponding to a particular DM particle mass, contributing to the observed DM relic density. Another interesting point is the exact vertical part of these lines in the region where PBH domination occurs. This lack of dependence on the PBH initial abundance is expected because in the case of PBH domination, the total energy density just before the standard RD phase is contributed only from the PBHs, and the fraction of DM energy density remains constant for a fixed mass DM particle. In the case when PBHs evaporate before they can dominate, the fraction of PBH contribution to the total energy density decreases, which also leads to a decrement in the DM energy density coming from PBHs.

We depend upon a few reasonable simplifying assumptions for the analytical estimate of present-day DM relic density contributed by PBH evaporation. The energy density of the DM particles evolves similarly to PBHs during PBH domination. For spin 1/2 particles, we effectively assume all the DM particles are produced instantly at the end of the PBH evaporation process as their production rate tends to peak at the very end [69]. If we consider the mass of the fermionic DM particle to be $m_{\text{DM}} \gg T_{\text{PBH},i}$, the total number of DM particles from a single BH can be approximated as [83],

$$N_{\text{DM}} \approx 7.27 \times 10^{33} g_{\text{DM}} \left(\frac{\text{GeV}}{m_{\text{DM}}} \right)^2. \quad (4.14)$$

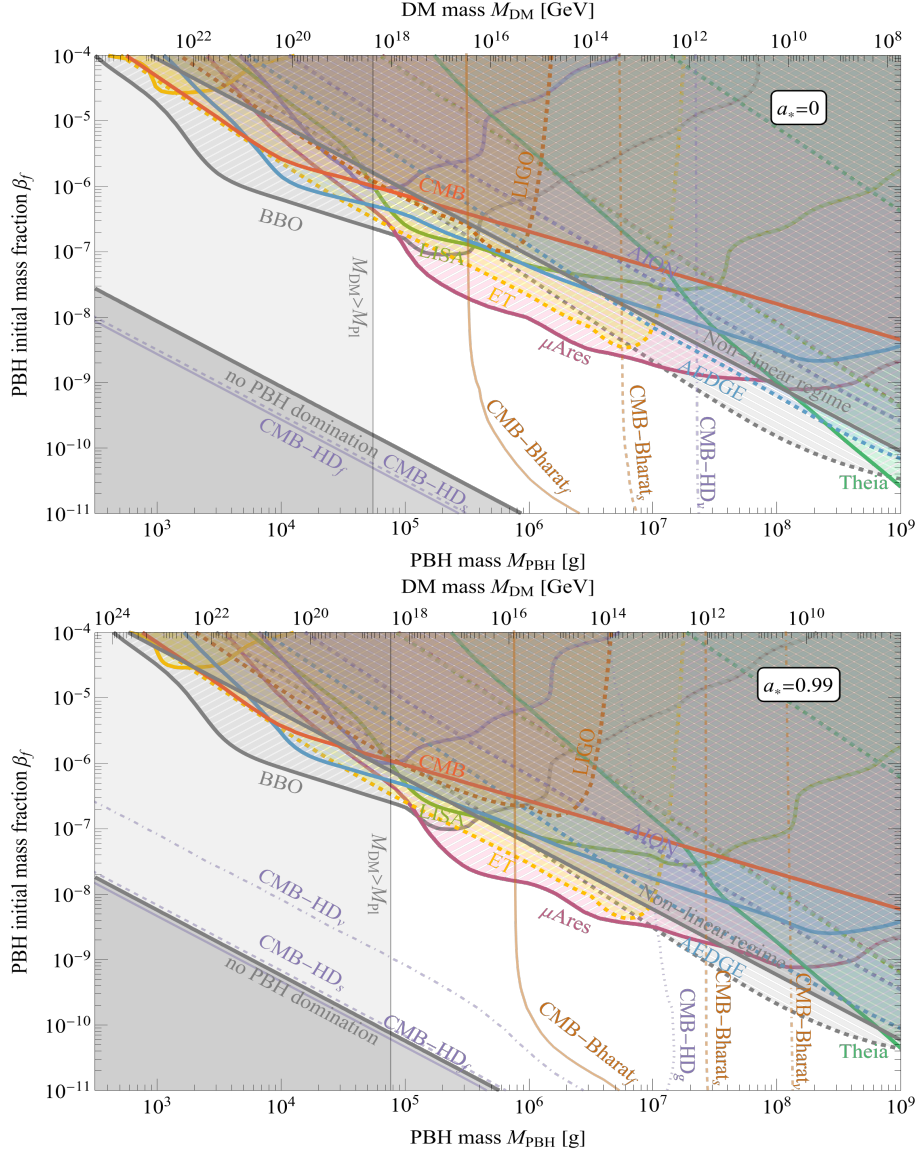


Figure (8) Filled contours indicate the spectra within the detection range of future GW experiments similar to Fig. 6. The top ticks indicate the mass of the DM relic leading to the correct abundance today. The top panel corresponds to $a_* = 0.0$, while in the lower panel, $a_* = 0.99$. Our DM results are only valid to the right of the vertical grey lines indicating $M_{\text{DM}} = M_{\text{Pl}}$. For contours denoted by CMB-HD or CMB-Bharat (without filling), the higher M_{PBH} and higher β_f region refers to the parameter-space where ΔN_{eff} from DR is within reach of future CMB experiments. We show scalar, fermionic, vector, or graviton DR contours indicated by the subscripts s, f, v , or g , respectively, just as in Fig. 6.

At the end of PBH evaporation which roughly contributes to DM energy density,

$$\rho_{\text{DM}}(\tau_r) = \rho_{\text{tot}}(\tau_r) \left(\frac{N_{\text{DM}} m_{\text{DM}}}{M_{\text{PBH}}} \right) \quad (4.15)$$

Translating it to the present-day energy density, we get

$$\rho_{\text{DM}}(\tau_0) = \rho_{\text{DM}}(\tau_r) \left(\frac{T_0}{T_r} \right)^3 \left(\frac{g_*(T_0)}{g_*(T_r)} \right) \quad (4.16)$$

and the present DM relic density of our universe comes out to be,

$$\Omega_{\text{DM}} = \frac{\rho_{\text{DM}}}{\rho_{\text{crit}}} \approx \left(\frac{g_{\text{DM}}}{g_{*,H}(T_r)} \right) \left(\frac{3.6 \times 10^9 \text{ GeV}}{m_{\text{DM}}} \right) \left(\frac{10^8 \text{ g}}{M_{\text{PBH}}} \right)^{5/2} (g_*(T_r))^{3/4}, \quad (4.17)$$

where we use the temperature of the universe at the end of PBH evaporation,

$$T_r \simeq 8.9 \times 10^7 \left(\frac{M_{\text{PBH}}}{10^2 \text{ g}} \right)^{-3/2} (g_*(T_r))^{-1/4} \text{ GeV}. \quad (4.18)$$

While this estimate is valid for non-spinning PBHs, it is tough to estimate N_{DM} analytically for spinning PBHs. From our results in section 4.1 that the emission of fermions stays nearly unaffected due to the change in initial PBH spin, we use this as an assumption to get an analytical estimation of Ω_{DM} for spinning PBHs. Taking $N_{\text{DM,spin}} \simeq N_{\text{DM,no-spin}}$, allows us to express,

$$\rho_{\text{DM,spin}}(\tau_0) \simeq \rho_{\text{DM,no-spin}}(\tau_0) \left(\frac{T_{r,\text{spin}}}{T_{r,\text{no-spin}}} \right), \quad (4.19)$$

and

$$\left(\frac{\Omega_{\text{DM,spin}}}{\Omega_{\text{DM,no-spin}}} \right) \approx \left(\frac{T_{r,\text{spin}}}{T_{r,\text{no-spin}}} \right) \approx \left(\frac{\Delta t_{\text{PBH,spin}}}{\Delta t_{\text{PBH}}^S} \right)^{-1/2} = \mathcal{F}(a_*)^{-1/2}. \quad (4.20)$$

It is also possible to get a significant abundance of DM particles even if we consider the scenario wherein the PBHs evaporate before they can dominate, as we can see in the lower part of the left panel of Fig. 7. Since our focus here is to connect DM with the observable ISGWB signals and we obtain amplification in the ISGWB spectrum only when there is a phase of PBH domination, for the analytical estimates, we limit ourselves to the parameter space where PBH can dominate the universe for a finite duration. Matching with the observed abundance of DM relic density provides us with a relation between the mass of PBHs and DM particle mass,

$$m_{\text{DM}} \approx 1.7 \times 10^5 \left(\frac{10^{10} \text{ g}}{M_{\text{PBH}}} \right)^{5/2} \mathcal{F}(a_*)^{-1/2} \text{ GeV}. \quad (4.21)$$

Using this expression, we plot m_{DM} as a function of M_{PBH} in the right panel of Fig. 7 along with the corresponding numerical values, which are obtained from scanning the parameter space where PBHs do dominate the universe for a finite period. The numerical and analytical results match quite closely, and we use the analytically derived m_{DM} in the upper bars of the upper and lower panel of Fig. 8 for $a_* = \{0.0, 0.99\}$. To complete the picture, we plot it along with the contours for detectable GW observations (with $\text{SNR} \geq 10$) and the CMB observation bounds for ΔN_{eff} for different particles species with $s = 0, 1/2, 1, 2$ as we have derived in the previous section.

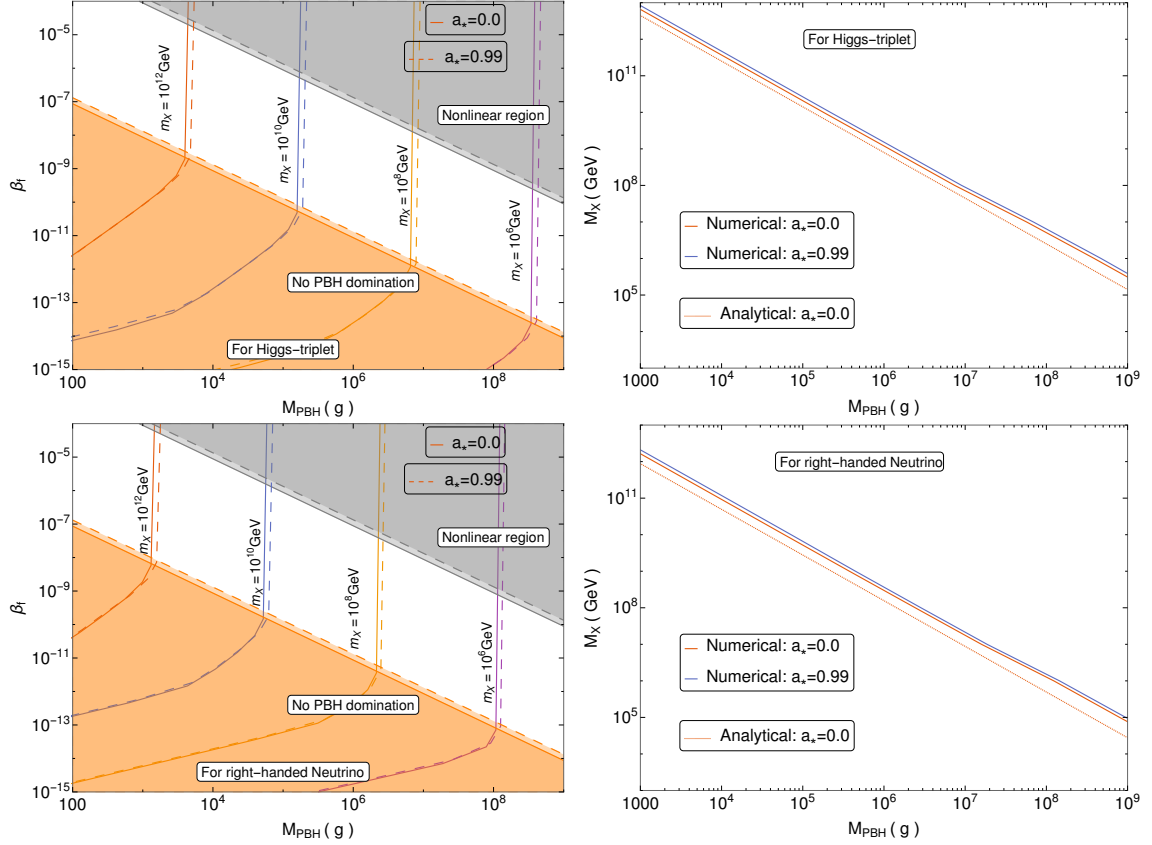


Figure (9) **Left panel:** We plot β_f as a function of M_{PBH} for the different masses of the heavy decaying particles, which contributes to the observed baryon asymmetry of our universe ($Y_B \approx 8.80 \times 10^{-11}$). The non-linear regime ($\tau_{\text{rat}} \geq 470$) is shaded in grey and no PBH domination in orange. **Right panel :** We set β_f such that we get an era of PBH domination and plot the mass of the heavy decaying particles which satisfy the baryon asymmetry observation. The comparison between the analytical and numerical results for non-spinning PBHs is reasonably good.

4.3 Baryogenesis

As we discussed in the previous section, massive non-relativistic stable particles emitted from Hawking evaporation of PBHs can lead to the DM component of our universe. On the other hand, if the emitted massive particles are unstable, they can decay in a baryon-number violating process which can contribute to the observed baryon asymmetry of our universe.

In our previous work [80], we considered PBH evaporation induced baryogenesis and connected the baryogenesis parameters with the PBH parameter space in the light of ISGWB observations. We considered two cases of baryogenesis: direct baryogenesis through the baryon-number violating decay of Higgs-triplets and baryogenesis through leptogenesis due to the decay of right-handed neutrinos and the subsequent conversion of lepton asymmetry to baryon asymmetry via the sphaleron processes. We assumed the baryogenesis scenario, where Higgs-triplet and right-handed neutrinos originate from Hawking evaporation of ultra-low mass PBHs. We denote the efficiency of the baryogenesis process with a parameter ϵ_X ,

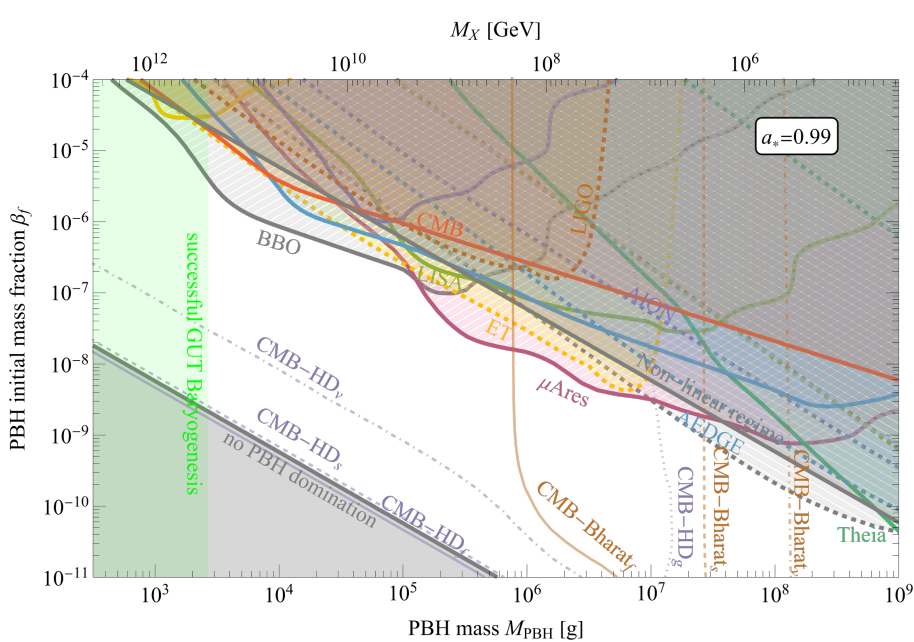


Figure (10) Reach of future GW observatories (filled contours) and CMB probes for DR (contours denoted by CMB-HD or CMB-Bharat, without filling) in terms of the mass and initial abundance of PBHs, just as in Fig. 8. The top panel corresponds to $a_* = 0.0$ while the lower is for $a_* = 0.99$. On the top axis, we indicate the mass of the Higgs triplet m_X for which we obtain the observed baryon asymmetry. The green shaded region corresponds to allowed regions for GUT baryogenesis from proton decay bound.

which can take different values up to unity depending on various decay channels and other factors in the baryogenesis process solely depending on the microphysics of the BSM particle

physics scenario under consideration. One can write an expression for ϵ_X in terms of the decay rate of particle model [76],

$$\epsilon_X \equiv \sum_i B_i \frac{\Gamma(X \rightarrow f_i) - \Gamma(\bar{X} \rightarrow \bar{f}_i)}{\Gamma_{\text{tot}}}, \quad (4.22)$$

where f_i is i^{th} final particle with baryon number B_i , and Γ_{tot} is the total decay width of the heavy particle. For the baryogenesis via leptogenesis scenario, we denote the conversion factor for lepton asymmetry to baryon asymmetry as $\lambda = 0.35$ [72].

In the present work, we revisit the same framework to include the effects of the initial spinning PBHs. For this purpose, we modify FRISBHEE to calculate the number density of the Higgs-triplet particle, $N_X(t_r)$ numerically at the end of PBH evaporation and estimate the total baryon asymmetry from Higgs-triplet particles as,

$$Y_B = \frac{n_{\text{PBH}}}{s(t_r)} \epsilon_X N_X = \left(\frac{N_X}{M_{\text{PBH}}} \right) \frac{\rho_{\text{tot}}(t_r)}{s(t_r)} \epsilon_X = \left(\frac{3}{4} \right) \left(\frac{N_X T_r}{M_{\text{PBH}}} \right) \frac{g_*(T_r)}{g_{*,S}(T_r)} \epsilon_X. \quad (4.23)$$

For Baryogenesis via leptogenesis mechanism with right-handed neutrinos, we need to include the conversion factor λ , and this formula gets modified to,

$$Y_B = \lambda \left(\frac{3}{4} \right) \left(\frac{N_X T_r}{M_{\text{PBH}}} \right) \frac{g_*(T_r)}{g_{*,S}(T_r)} \epsilon_X. \quad (4.24)$$

In the left panels of Fig. 9, we use the exact numerical setup and plot the lines connecting the points of PBH parameter space which are found to produce the observed baryogenesis for a particular mass of decaying particles, Higgs-triplet (upper panel) and right-handed neutrinos (lower panel). For the case of PBH domination, we find the estimated baryon asymmetry to have negligible dependence on initial PBH abundance β_f , which is qualitatively similar to the DM and DR scenario. Using $Y_B \approx 8.8 \times 10^{-11}$ (inferred from CMB observations [145, 151] and BBN constraints [152, 153]) and $\epsilon_X = 1$, we get an analytical relation between the initial PBH mass M_{PBH} and mass of the decaying heavy particle M_X as [80],

$$M_X \approx 2.5 \times 10^{16} \sqrt{\epsilon_X \left(\frac{1 \text{ g}}{M_{\text{PBH}}} \right)^{5/2}} \text{ GeV} \quad (\text{For Higgs-triplet in GUT baryogenesis}). \quad (4.25)$$

$$M_X \approx 5.9 \times 10^{15} \sqrt{\epsilon_X \left(\frac{1 \text{ g}}{M_{\text{PBH}}} \right)^{5/2}} \text{ GeV} \quad (\text{For right-handed neutrinos}). \quad (4.26)$$

In the right panels of Fig. 9, we plot these approximate analytical results for the Schwarzschild case, along with the numerically obtained mass of the Higgs-triplet (upper panel) and right-handed neutrinos (lower panel) as a function of M_{PBH} which leads to observed matter-antimatter asymmetry, both for initially spinning and non-spinning population of PBHs. We find a negligible deviation from non-spinning results to spinning PBHs, while the mismatch between numerical and analytical results is somewhat significant.

As we are considering scalar Higgs-triplet particles in the GUT baryogenesis context and right-handed neutrinos in case of baryogenesis via leptogenesis scenario and the emission of $s = 0$ and $s = 1/2$ particles get negligibly affected due to the inclusion of spin, a very weak dependence on the initial PBH spin is expected. Using our analytical Schwarzschild expression, we plot the corresponding mass ranges m_X of Higgs triplet particles in the upper

panel of Fig. 10. We also plot the proton decay bound in the green vertical contours for direct GUT baryogenesis models as required by the laboratory constraints on proton decay from SuperK experiment [154] and take the efficiency parameter $\epsilon_X = 1$ for all our calculations. The lower panel of Fig. 10 show similar contours for spinning PBHs with $a_* = 0.99$. It is interesting to note the comparative difference in the ISGWB detection possibility lines in the two plots for two different values of the spin parameter a_* . However, the predictions from baryogenesis remain nearly the same. It is important to note that we only plot the mass range of Higgs-triplet particles for direct baryogenesis in the upper panel of Fig. 10, which is not valid for right-handed neutrinos. We plot it as a representative plot to illustrate the combined picture of ISGWB detection probability, detectable DR parameter space, and baryogenesis scenario.

5 Conclusions and discussions

In this paper, we have explored diverse observational consequences of an early scenario populated by ultra-low mass PBHs, which briefly dominate the energy density of the universe but evaporate before BBN. There are several important implications of such a scenario; for instance, the emitted byproducts from PBHs, depending on their properties, can contribute to the DM energy density, additional DR contribution and baryogenesis via the decay of unstable particles. In this work, we study how these different aspects can complement each other, and a combination of them, as a whole, can offer a better understanding of the post-inflationary phase before BBN. In our earlier work [80], we studied the origin of a doubly-peaked ISGWB in such a scenario which can be used as a novel tool to probe such a possibility. Here, we have extended the scope of our earlier work by including the initially spinning PBHs and quantitatively identified the corresponding signatures in DR, DM, and baryogenesis with the help of an exact numerical setup. Some interesting findings of our work can be summarized below:

- The resonant ISGWB spectrum of a unique doubly-peaked shape contributed from the isocurvature-induced adiabatic perturbations associated with the PBHs distribution and from the inflationary adiabatic scalar perturbations can be detected with various future GWs detectors (see, Figs. 6 and 8) and can also be used to constrain the PBH parameter space from the results on N_{eff} from the existing CMB observations. For the ISGWB, the primary effect of including the initially spinning PBHs arises from the modified PBH lifetime. PBHs with non-zero spin evaporate more rapidly, and that change in the evaporation timescale results in the modification of the ISGWB spectrum as shown in Figs. 2 and 3. The peak frequency and the height of the peak both get modified slightly, which shows a weak dependence of ISGWB on the PBH spin.
- While the PBH spin does not play a significant role in the ISGWB signal, in the case of the DR from Hawking evaporation, the effect of initially spinning PBHs varies depending on the type of emitted particle, as we can see from Figs. 4 and 5, from scalar particles, larger PBH spin results in smaller ΔN_{eff} and reduced detectability, but as we go for higher spin DR particles like the graviton, the larger PBH spin is found to contribute significantly to ΔN_{eff} , thereby, enhancing the detectability. This characteristic feature of gravitons opens up an exciting possibility of detecting the initial PBH spin through DR in future CMB observations like CMB-HD and CMB-Bharat. As evident from Fig. 6, we obtain a PBH mass-dependent cutoff value of PBH spin, only

above which ΔN_{eff} from the graviton becomes detectable in the CMB-HD experiment. Though the sensitivity of PBH spin is weaker in the case of vector particles compared to the graviton, similar behaviour for the ΔN_{eff} detectable in CMB-HD is also visible for vector particles.

- Non-thermal production of DM candidates satisfying the observed relic density is notoriously challenging to test in DM laboratory experiments due to the null interactions with the standard model as well as the high energy scales involved. However, the doubly-peaked ISGWB spectrum allows us to probe such DM production with varying DM masses, as shown in Figs. 7 and 8. Considering Dirac fermions as DM particles, we find the dependence of PBH spin to be very weak. Similarly, for PBH-induced baryogenesis, we find a very weak PBH spin sensitivity both for direct baryogenesis and baryogenesis via leptogenesis scenario, as evident from Fig. 9.
- Though initial PBH spin leaves insignificant effects in the case of ISGWB, fermionic DM, and scalar vector and fermionic DR particles, we find significant effects of PBH spin for graviton as DR particles. It offers us an exciting opportunity to employ otherwise unrelated experiments, CMB detectors, and GW detectors to break the degeneracy between spinning and nonspinning PBH scenarios. Thus, cosmological estimations of ΔN_{eff} from CMB experiments and detection of ISGWB in future GW observations complement each other (see Fig. 7) to constrain the reheating history more effectively.
- Different observational probes offer very different sensitivities for initial PBH abundance, β_f . As we have discussed, ISGWB strongly depends on the initial PBH abundance, as even a slight change in β_f alters the duration of the early PBH domination and leads to large modifications of the ISGWB peaks. On the other hand, when we consider scenarios with the generation of DR, DM or baryogenesis from Hawking evaporation, we find them to depend on β_f only when PBHs evaporate before they can dominate the universe. But, if the PBHs dominate the universe for a finite duration, the initial abundance of PBH or the duration of PBH domination does not alter the results significantly, as is evident from the left panels of Figs. 7 and 9, and also from the sensitivity plots in Figs. 8 and 10.

To conclude, Hawking evaporation of a dominant population of ultra-low mass spinning and non-spinning PBHs can lead to cosmological relics such as DM, DR, and baryon asymmetry, and the doubly-peaked ISGWB arising inevitably in such a scenario can potentially probe and constrain these contributions. We have exhibited a novel complementarity of different probes like the future CMB experiments and GW detectors and found the synergy of future GW observatories and CMB missions to observe ΔN_{eff} to put very strong constraints on PBH parameter space as well as the reheating history of the pre-BBN universe.

There have been some recent efforts to include more realistic non-monochromatic PBH mass distribution, both in the context of ISGWB [113] and on the Hawking evaporation-induced baryogenesis [155]. In a similar context, it would also be interesting to explore the effects of the non-monochromatic spin distribution of ultra-low mass PBHs and resulting modifications in ISGWB, dark sector and baryogenesis. Taking into account the clustering of PBHs during the eMD epoch and different spatial distributions of PBHs are also expected to leave imprints on our results, particularly on the ISGWB part, which we leave for future work. We do not work with any PBH-forming models for the inflationary adiabatic perturbations.

Instead, we use the standard power-law power spectrum on all scales. If we consider specific inflationary models for the formation of such ultra-low mass PBHs, our estimation of the ISGWB near the PBH forming scales is expected to be modified, which would be interesting to explore further. A prolonged eMD phase also restricts the allowed number of e-folds from the horizon exit of the CMB pivot scale to the end of inflation [156]. This constraint, along with the optimal range of the scalar spectral index n_s and the tensor to scalar ratio r from CMB observations [122] allows one to put constraints on possible inflationary models. For an early PBH domination, such an analysis would allow us to constrain the PBH parameter space directly and, thereby, check the consistency of the Hawking evaporation-driven baryogenesis and DM production, for a particular model of inflation. We leave it for future work.

Acknowledgments

The authors thank Lucien Heurtier for useful discussions and suggestions about FRISBHEE. NB thanks Yashi Tiwari, Ranjan Laha, and Akash Kumar Saha for helpful discussions and suggestions. This work was supported by the Polish National Agency for Academic Exchange within Polish Returns Programme under agreement PPN/PPO/2020/1/00013/U/00001 and the Polish National Science Center grant 2018/31/D/ST2/02048. RKJ acknowledges financial support from the new faculty seed start-up grant of the Indian Institute of Science, Bengaluru; Science and Engineering Research Board, Department of Science and Technology, Govt. of India, through the Core Research Grant CRG/2018/002200 and the Infosys Foundation, Bengaluru, India, through the Infosys Young Investigator Award.

References

- [1] Y. B. Zel’dovich and I. D. Novikov, *The Hypothesis of Cores Retarded during Expansion and the Hot Cosmological Model*, *Soviet Astronomy* **10** (Jan., 1967) 602.
- [2] S. Hawking, *Gravitationally collapsed objects of very low mass*, *Mon. Not. Roy. Astron. Soc.* **152** (1971) 75.
- [3] B. J. Carr and S. W. Hawking, *Black holes in the early Universe*, *Mon. Not. Roy. Astron. Soc.* **168** (1974) 399–415.
- [4] B. J. Carr, *The Primordial black hole mass spectrum*, *Astrophys. J.* **201** (1975) 1–19.
- [5] G. F. Chapline, *Cosmological effects of primordial black holes*, *Nature* **253** (1975), no. 5489 251–252.
- [6] B. Carr, S. Clesse, J. García-Bellido, and F. Kühnel, *Cosmic conundra explained by thermal history and primordial black holes*, *Phys. Dark Univ.* **31** (2021) 100755, [[arXiv:1906.08217](#)].
- [7] A. Escrivà, F. Kuhnel, and Y. Tada, *Primordial Black Holes*, [[arXiv:2211.05767](#)].
- [8] S. Bird, I. Cholis, J. B. Muñoz, Y. Ali-Haïmoud, M. Kamionkowski, E. D. Kovetz, A. Raccanelli, and A. G. Riess, *Did LIGO detect dark matter?*, *Phys. Rev. Lett.* **116** (2016), no. 20 201301, [[arXiv:1603.00464](#)].
- [9] **LIGO Scientific, Virgo** Collaboration, B. P. Abbott et al., *Observation of Gravitational Waves from a Binary Black Hole Merger*, *Phys. Rev. Lett.* **116** (2016), no. 6 061102, [[arXiv:1602.03837](#)].
- [10] **LIGO Scientific, Virgo** Collaboration, R. Abbott et al., *GW190521: A Binary Black Hole Merger with a Total Mass of $150M_{\odot}$* , *Phys. Rev. Lett.* **125** (2020), no. 10 101102, [[arXiv:2009.01075](#)].

- [11] **LIGO Scientific, Virgo** Collaboration, B. P. Abbott et al., *Observation of Gravitational Waves from a Binary Black Hole Merger*, *Phys. Rev. Lett.* **116** (2016), no. 6 061102, [[arXiv:1602.03837](#)].
- [12] **LIGO Scientific, Virgo** Collaboration, B. P. Abbott et al., *GW151226: Observation of Gravitational Waves from a 22-Solar-Mass Binary Black Hole Coalescence*, *Phys. Rev. Lett.* **116** (2016), no. 24 241103, [[arXiv:1606.04855](#)].
- [13] **LIGO Scientific, Virgo** Collaboration, B. P. Abbott et al., *GW170104: Observation of a 50-Solar-Mass Binary Black Hole Coalescence at Redshift 0.2*, *Phys. Rev. Lett.* **118** (2017), no. 22 221101, [[arXiv:1706.01812](#)]. [Erratum: *Phys. Rev. Lett.* 121, no. 12, 129901 (2018)].
- [14] S. Clesse and J. García-Bellido, *Detecting the gravitational wave background from primordial black hole dark matter*, *Phys. Dark Univ.* **18** (2017) 105–114, [[arXiv:1610.08479](#)].
- [15] G. Hütsi, M. Raidal, V. Vaskonen, and H. Veermäe, *Two populations of LIGO-Virgo black holes*, *JCAP* **03** (2021) 068, [[arXiv:2012.02786](#)].
- [16] B. Carr, K. Kohri, Y. Sendouda, and J. Yokoyama, *Constraints on primordial black holes*, *Rept. Prog. Phys.* **84** (2021), no. 11 116902, [[arXiv:2002.12778](#)].
- [17] B. J. Carr, K. Kohri, Y. Sendouda, and J. Yokoyama, *Constraints on primordial black holes from the Galactic gamma-ray background*, *Phys. Rev.* **D94** (2016), no. 4 044029, [[arXiv:1604.05349](#)].
- [18] A. Barnacka, J. F. Glicenstein, and R. Moderski, *New constraints on primordial black holes abundance from femtolensing of gamma-ray bursts*, *Phys. Rev.* **D86** (2012) 043001, [[arXiv:1204.2056](#)].
- [19] R. Laha, *Primordial Black Holes as a Dark Matter Candidate Are Severely Constrained by the Galactic Center 511 keV γ -Ray Line*, *Phys. Rev. Lett.* **123** (2019), no. 25 251101, [[arXiv:1906.09994](#)].
- [20] H. Niikura et al., *Microlensing constraints on primordial black holes with Subaru/HSC Andromeda observations*, *Nat. Astron.* **3** (2019), no. 6 524–534, [[arXiv:1701.02151](#)].
- [21] **EROS-2** Collaboration, P. Tisserand et al., *Limits on the Macho Content of the Galactic Halo from the EROS-2 Survey of the Magellanic Clouds*, *Astron. Astrophys.* **469** (2007) 387–404, [[astro-ph/0607207](#)].
- [22] H. Niikura, M. Takada, S. Yokoyama, T. Sumi, and S. Masaki, *Constraints on Earth-mass primordial black holes from OGLE 5-year microlensing events*, *Phys. Rev.* **D99** (2019), no. 8 083503, [[arXiv:1901.07120](#)].
- [23] M. Ricotti, J. P. Ostriker, and K. J. Mack, *Effect of Primordial Black Holes on the Cosmic Microwave Background and Cosmological Parameter Estimates*, *Astrophys. J.* **680** (2008) 829, [[arXiv:0709.0524](#)].
- [24] D. Aloni, K. Blum, and R. Flauger, *Cosmic microwave background constraints on primordial black hole dark matter*, *JCAP* **05** (2017) 017, [[arXiv:1612.06811](#)].
- [25] V. Poulin, P. D. Serpico, F. Calore, S. Clesse, and K. Kohri, *CMB bounds on disk-accreting massive primordial black holes*, *Phys. Rev.* **D96** (2017), no. 8 083524, [[arXiv:1707.04206](#)].
- [26] A. K. Saha and R. Laha, *Sensitivities on non-spinning and spinning primordial black hole dark matter with global 21 cm troughs*, [[arXiv:2112.10794](#)].
- [27] S. Mittal, A. Ray, G. Kulkarni, and B. Dasgupta, *Constraining primordial black holes as dark matter using the global 21-cm signal with X-ray heating and excess radio background*, *JCAP* **03** (2022) 030, [[arXiv:2107.02190](#)].
- [28] K. Kohri, T. Sekiguchi, and S. Wang, *Cosmological 21cm line observations to test scenarios of super-Eddington accretion on to black holes being seeds of high-redshifted supermassive black*

holes, [arXiv:2201.05300](#).

- [29] G. Hasinger, *Illuminating the dark ages: Cosmic backgrounds from accretion onto primordial black hole dark matter*, *JCAP* **07** (2020) 022, [[arXiv:2003.05150](#)].
- [30] H. Tashiro and N. Sugiyama, *The effect of primordial black holes on 21 cm fluctuations*, *Mon. Not. Roy. Astron. Soc.* **435** (2013) 3001, [[arXiv:1207.6405](#)].
- [31] A. Hektor, G. Hütsi, L. Marzola, M. Raidal, V. Vaskonen, and H. Veermäe, *Constraining Primordial Black Holes with the EDGES 21-cm Absorption Signal*, *Phys. Rev. D* **98** (2018), no. 2 023503, [[arXiv:1803.09697](#)].
- [32] P. Montero-Camacho, X. Fang, G. Vasquez, M. Silva, and C. M. Hirata, *Revisiting constraints on asteroid-mass primordial black holes as dark matter candidates*, *JCAP* **08** (2019) 031, [[arXiv:1906.05950](#)].
- [33] N. Bhaumik and R. K. Jain, *Primordial black holes dark matter from inflection point models of inflation and the effects of reheating*, *JCAP* **01** (2020) 037, [[arXiv:1907.04125](#)].
- [34] J. Garcia-Bellido and E. Ruiz Morales, *Primordial black holes from single field models of inflation*, *Phys. Dark Univ.* **18** (2017) 47–54, [[arXiv:1702.03901](#)].
- [35] M. P. Hertzberg and M. Yamada, *Primordial Black Holes from Polynomial Potentials in Single Field Inflation*, *Phys. Rev.* **D97** (2018), no. 8 083509, [[arXiv:1712.09750](#)].
- [36] G. Ballesteros and M. Taoso, *Primordial black hole dark matter from single field inflation*, *Phys. Rev.* **D97** (2018), no. 2 023501, [[arXiv:1709.05565](#)].
- [37] H. Ragavendra, P. Saha, L. Sriramkumar, and J. Silk, *PBHs and secondary GWs from ultra slow roll and punctuated inflation*, [arXiv:2008.12202](#).
- [38] S. S. Mishra and V. Sahni, *Primordial Black Holes from a tiny bump/dip in the Inflaton potential*, *JCAP* **04** (2020) 007, [[arXiv:1911.00057](#)].
- [39] R. Arya, *Formation of Primordial Black Holes from Warm Inflation*, *JCAP* **09** (2020) 042, [[arXiv:1910.05238](#)].
- [40] M. Bastero-Gil and M. S. Díaz-Blanco, *Gravity waves and primordial black holes in scalar warm little inflation*, *JCAP* **12** (2021), no. 12 052, [[arXiv:2105.08045](#)].
- [41] R. Arya, R. K. Jain, and A. K. Mishra, *Primordial Black Holes Dark Matter and Secondary Gravitational Waves from Warm Higgs-G Inflation*, [arXiv:2302.08940](#).
- [42] S. Kawai and J. Kim, *Primordial black holes from Gauss-Bonnet-corrected single field inflation*, *Phys. Rev. D* **104** (2021), no. 8 083545, [[arXiv:2108.01340](#)].
- [43] M. Braglia, D. K. Hazra, F. Finelli, G. F. Smoot, L. Sriramkumar, and A. A. Starobinsky, *Generating PBHs and small-scale GWs in two-field models of inflation*, *JCAP* **08** (2020) 001, [[arXiv:2005.02895](#)].
- [44] L. Anguelova, *On Primordial Black Holes from Rapid Turns in Two-field Models*, *JCAP* **06** (2021) 004, [[arXiv:2012.03705](#)].
- [45] S. Clesse and J. Garcia-Bellido, *Massive Primordial Black Holes from Hybrid Inflation as Dark Matter and the seeds of Galaxies*, *Phys. Rev.* **D92** (2015), no. 2 023524, [[arXiv:1501.07565](#)].
- [46] S. W. Hawking, I. G. Moss, and J. M. Stewart, *Bubble Collisions in the Very Early Universe*, *Phys. Rev. D* **26** (1982) 2681.
- [47] H. Kodama, M. Sasaki, and K. Sato, *Abundance of Primordial Holes Produced by Cosmological First Order Phase Transition*, *Prog. Theor. Phys.* **68** (1982) 1979.
- [48] K. Jedamzik and J. C. Niemeyer, *Primordial black hole formation during first order phase transitions*, *Phys. Rev.* **D59** (1999) 124014, [[astro-ph/9901293](#)].

- [49] M. Lewicki and V. Vaskonen, *On bubble collisions in strongly supercooled phase transitions*, *Phys. Dark Univ.* **30** (2020) 100672, [[arXiv:1912.00997](#)].
- [50] S. W. Hawking, *Black Holes From Cosmic Strings*, *Phys. Lett. B* **231** (1989) 237–239.
- [51] A. Polnarev and R. Zembowicz, *Formation of Primordial Black Holes by Cosmic Strings*, *Phys. Rev. D* **43** (1991) 1106–1109.
- [52] J. H. MacGibbon, R. H. Brandenberger, and U. F. Wichoski, *Limits on black hole formation from cosmic string loops*, *Phys. Rev. D* **57** (1998) 2158–2165, [[astro-ph/9707146](#)].
- [53] S. G. Rubin, M. Y. Khlopov, and A. S. Sakharov, *Primordial black holes from nonequilibrium second order phase transition*, *Grav. Cosmol.* **6** (2000) 51–58, [[hep-ph/0005271](#)].
- [54] S. G. Rubin, A. S. Sakharov, and M. Y. Khlopov, *The Formation of primary galactic nuclei during phase transitions in the early universe*, *J. Exp. Theor. Phys.* **91** (2001) 921–929, [[hep-ph/0106187](#)].
- [55] R. Brandenberger, B. Cyr, and H. Jiao, *Intermediate Mass Black Hole Seeds from Cosmic String Loops*, [arXiv:2103.14057](#).
- [56] E. Cotner and A. Kusenko, *Primordial black holes from supersymmetry in the early universe*, *Phys. Rev. Lett.* **119** (2017), no. 3 031103, [[arXiv:1612.02529](#)].
- [57] T. Suyama, T. Tanaka, B. Bassett, and H. Kudoh, *Are black holes over-produced during preheating?*, *Phys. Rev. D* **71** (2005) 063507, [[hep-ph/0410247](#)].
- [58] T. Suyama, T. Tanaka, B. Bassett, and H. Kudoh, *Black hole production in tachyonic preheating*, *JCAP* **0604** (2006) 001, [[hep-ph/0601108](#)].
- [59] B. A. Bassett and S. Tsujikawa, *Inflationary preheating and primordial black holes*, *Phys. Rev. D* **63** (2001) 123503, [[hep-ph/0008328](#)].
- [60] J. Martin, T. Papanikolaou, and V. Vennin, *Primordial black holes from the preheating instability in single-field inflation*, *JCAP* **01** (2020) 024, [[arXiv:1907.04236](#)].
- [61] J. Martin, T. Papanikolaou, L. Pinol, and V. Vennin, *Metric preheating and radiative decay in single-field inflation*, *JCAP* **05** (2020) 003, [[arXiv:2002.01820](#)].
- [62] G. Dvali, F. Kühnel, and M. Zantedeschi, *Primordial black holes from confinement*, *Phys. Rev. D* **104** (2021), no. 12 123507, [[arXiv:2108.09471](#)].
- [63] B. J. Carr, K. Kohri, Y. Sendouda, and J. Yokoyama, *New cosmological constraints on primordial black holes*, *Phys. Rev. D* **81** (2010) 104019, [[arXiv:0912.5297](#)].
- [64] C. Keith, D. Hooper, N. Blinov, and S. D. McDermott, *Constraints on Primordial Black Holes From Big Bang Nucleosynthesis Revisited*, *Phys. Rev. D* **102** (2020), no. 10 103512, [[arXiv:2006.03608](#)].
- [65] B. Carr and F. Kühnel, *Primordial Black Holes as Dark Matter: Recent Developments*, *Ann. Rev. Nucl. Part. Sci.* **70** (2020) 355–394, [[arXiv:2006.02838](#)].
- [66] D. Hooper, G. Krnjaic, and S. D. McDermott, *Dark Radiation and Superheavy Dark Matter from Black Hole Domination*, *JHEP* **08** (2019) 001, [[arXiv:1905.01301](#)].
- [67] C. Lunardini and Y. F. Perez-Gonzalez, *Dirac and Majorana neutrino signatures of primordial black holes*, *JCAP* **08** (2020) 014, [[arXiv:1910.07864](#)].
- [68] I. Masina, *Dark matter and dark radiation from evaporating primordial black holes*, *Eur. Phys. J. Plus* **135** (2020), no. 7 552, [[arXiv:2004.04740](#)].
- [69] I. Masina, *Dark Matter and Dark Radiation from Evaporating Kerr Primordial Black Holes*, *Grav. Cosmol.* **27** (2021), no. 4 315–330, [[arXiv:2103.13825](#)].
- [70] A. Arbey, J. Auffinger, P. Sandick, B. Shams Es Haghi, and K. Sinha, *Precision calculation of*

dark radiation from spinning primordial black holes and early matter-dominated eras, *Phys. Rev. D* **103** (2021), no. 12 123549, [[arXiv:2104.04051](#)].

- [71] D. Baumann, P. J. Steinhardt, and N. Turok, *Primordial Black Hole Baryogenesis*, [hep-th/0703250](#).
- [72] T. Fujita, M. Kawasaki, K. Harigaya, and R. Matsuda, *Baryon asymmetry, dark matter, and density perturbation from primordial black holes*, *Phys. Rev. D* **89** (2014), no. 10 103501, [[arXiv:1401.1909](#)].
- [73] A. Hook, *Baryogenesis from Hawking Radiation*, *Phys. Rev. D* **90** (2014), no. 8 083535, [[arXiv:1404.0113](#)].
- [74] Y. Hamada and S. Iso, *Baryon asymmetry from primordial black holes*, *PTEP* **2017** (2017), no. 3 033B02, [[arXiv:1610.02586](#)].
- [75] A. Chaudhuri and A. Dolgov, *PBH Evaporation, Baryon Asymmetry, and Dark Matter*, *J. Exp. Theor. Phys.* **133** (2021), no. 5 552–566, [[arXiv:2001.11219](#)].
- [76] D. Hooper and G. Krnjaic, *GUT Baryogenesis With Primordial Black Holes*, *Phys. Rev. D* **103** (2021), no. 4 043504, [[arXiv:2010.01134](#)].
- [77] Y. F. Perez-Gonzalez and J. Turner, *Assessing the tension between a black hole dominated early universe and leptogenesis*, *Phys. Rev. D* **104** (2021), no. 10 103021, [[arXiv:2010.03565](#)].
- [78] S. Datta, A. Ghosal, and R. Samanta, *Baryogenesis from ultralight primordial black holes and strong gravitational waves from cosmic strings*, *JCAP* **08** (2021) 021, [[arXiv:2012.14981](#)].
- [79] S. Jyoti Das, D. Mahanta, and D. Borah, *Low scale leptogenesis and dark matter in the presence of primordial black holes*, *JCAP* **11** (2021) 019, [[arXiv:2104.14496](#)].
- [80] N. Bhaumik, A. Ghoshal, and M. Lewicki, *Doubly peaked induced stochastic gravitational wave background: testing baryogenesis from primordial black holes*, *JHEP* **07** (2022) 130, [[arXiv:2205.06260](#)].
- [81] N. F. Bell and R. R. Volkas, *Mirror matter and primordial black holes*, *Phys. Rev. D* **59** (1999) 107301, [[astro-ph/9812301](#)].
- [82] R. Allahverdi, J. Dent, and J. Osinski, *Nonthermal production of dark matter from primordial black holes*, *Phys. Rev. D* **97** (2018), no. 5 055013, [[arXiv:1711.10511](#)].
- [83] O. Lennon, J. March-Russell, R. Petrossian-Byrne, and H. Tillim, *Black Hole Genesis of Dark Matter*, *JCAP* **04** (2018) 009, [[arXiv:1712.07664](#)].
- [84] L. Morrison, S. Profumo, and Y. Yu, *Melanopogenesis: Dark Matter of (almost) any Mass and Baryonic Matter from the Evaporation of Primordial Black Holes weighing a Ton (or less)*, *JCAP* **05** (2019) 005, [[arXiv:1812.10606](#)].
- [85] P. Gondolo, P. Sandick, and B. Shams Es Haghi, *Effects of primordial black holes on dark matter models*, *Phys. Rev. D* **102** (2020), no. 9 095018, [[arXiv:2009.02424](#)].
- [86] N. Bernal and O. Zapata, *Self-interacting Dark Matter from Primordial Black Holes*, *JCAP* **03** (2021) 007, [[arXiv:2010.09725](#)].
- [87] N. Bernal and O. Zapata, *Dark Matter in the Time of Primordial Black Holes*, *JCAP* **03** (2021) 015, [[arXiv:2011.12306](#)].
- [88] N. Bernal and O. Zapata, *Gravitational dark matter production: primordial black holes and UV freeze-in*, *Phys. Lett. B* **815** (2021) 136129, [[arXiv:2011.02510](#)].
- [89] T. Kitabayashi, *Primordial black holes and scotogenic dark matter*, *Int. J. Mod. Phys. A* **36** (2021), no. 18 2150139, [[arXiv:2101.01921](#)].
- [90] A. Cheek, L. Heurtier, Y. F. Perez-Gonzalez, and J. Turner, *Primordial black hole evaporation and dark matter production. I. Solely Hawking radiation*, *Phys. Rev. D* **105** (2022), no. 1

015022, [[arXiv:2107.00013](#)].

- [91] A. Cheek, L. Heurtier, Y. F. Perez-Gonzalez, and J. Turner, *Primordial black hole evaporation and dark matter production. II. Interplay with the freeze-in or freeze-out mechanism*, *Phys. Rev. D* **105** (2022), no. 1 015023, [[arXiv:2107.00016](#)].
- [92] B. Barman, D. Borah, S. Jyoti Das, and R. Roshan, *Gravitational wave signatures of PBH-generated baryon-dark matter coincidence*, [arXiv:2212.00052](#).
- [93] D. Borah, S. Jyoti Das, R. Samanta, and F. R. Urban, *PBH-infused seesaw origin of matter and unique gravitational waves*, [arXiv:2211.15726](#).
- [94] Y. Ali-Haïmoud, E. D. Kovetz, and M. Kamionkowski, *Merger rate of primordial black-hole binaries*, *Phys. Rev. D* **96** (2017), no. 12 123523, [[arXiv:1709.06576](#)].
- [95] K. Kohri and T. Terada, *Primordial Black Hole Dark Matter and LIGO/Virgo Merger Rate from Inflation with Running Spectral Indices: Formation in the Matter- and/or Radiation-Dominated Universe*, *Class. Quant. Grav.* **35** (2018), no. 23 235017, [[arXiv:1802.06785](#)].
- [96] M. Raidal, C. Spethmann, V. Vaskonen, and H. Veermäe, *Formation and Evolution of Primordial Black Hole Binaries in the Early Universe*, *JCAP* **02** (2019) 018, [[arXiv:1812.01930](#)].
- [97] A. D. Gow, C. T. Byrnes, A. Hall, and J. A. Peacock, *Primordial black hole merger rates: distributions for multiple LIGO observables*, *JCAP* **01** (2020) 031, [[arXiv:1911.12685](#)].
- [98] K. Jedamzik, *Consistency of Primordial Black Hole Dark Matter with LIGO/Virgo Merger Rates*, *Phys. Rev. Lett.* **126** (2021), no. 5 051302, [[arXiv:2007.03565](#)].
- [99] E. Bagui and S. Clesse, *A boosted gravitational wave background for primordial black holes with broad mass distributions and thermal features*, *Phys. Dark Univ.* **38** (2022) 101115, [[arXiv:2110.07487](#)].
- [100] R. Saito and J. Yokoyama, *Gravitational wave background as a probe of the primordial black hole abundance*, *Phys. Rev. Lett.* **102** (2009) 161101, [[arXiv:0812.4339](#)]. [Erratum: *Phys.Rev.Lett.* 107, 069901 (2011)].
- [101] K. Kohri and T. Terada, *Semianalytic calculation of gravitational wave spectrum nonlinearly induced from primordial curvature perturbations*, *Phys. Rev. D* **97** (2018), no. 12 123532, [[arXiv:1804.08577](#)].
- [102] J. R. Espinosa, D. Racco, and A. Riotto, *A Cosmological Signature of the SM Higgs Instability: Gravitational Waves*, *JCAP* **09** (2018) 012, [[arXiv:1804.07732](#)].
- [103] G. Domènech, *Scalar Induced Gravitational Waves Review*, *Universe* **7** (2021), no. 11 398, [[arXiv:2109.01398](#)].
- [104] A. Ashoorioon, A. Rostami, and J. T. Firouzjaee, *Examining the end of inflation with primordial black holes mass distribution and gravitational waves*, *Phys. Rev. D* **103** (2021) 123512, [[arXiv:2012.02817](#)].
- [105] A. Ashoorioon, K. Rezazadeh, and A. Rostami, *NANOGrav signal from the end of inflation and the LIGO mass and heavier primordial black holes*, *Phys. Lett. B* **835** (2022) 137542, [[arXiv:2202.01131](#)].
- [106] R.-g. Cai, S. Pi, and M. Sasaki, *Gravitational Waves Induced by non-Gaussian Scalar Perturbations*, *Phys. Rev. Lett.* **122** (2019), no. 20 201101, [[arXiv:1810.11000](#)].
- [107] A. D. Dolgov and D. Ejlli, *Relic gravitational waves from light primordial black holes*, *Phys. Rev. D* **84** (2011) 024028, [[arXiv:1105.2303](#)].
- [108] K. Inomata, K. Kohri, T. Nakama, and T. Terada, *Enhancement of Gravitational Waves Induced by Scalar Perturbations due to a Sudden Transition from an Early Matter Era to the*

- Radiation Era*, *Phys. Rev. D* **100** (2019), no. 4 043532, [[arXiv:1904.12879](#)].
- [109] K. Inomata, M. Kawasaki, K. Mukaida, T. Terada, and T. T. Yanagida, *Gravitational Wave Production right after a Primordial Black Hole Evaporation*, *Phys. Rev. D* **101** (2020), no. 12 123533, [[arXiv:2003.10455](#)].
 - [110] G. Domènech, C. Lin, and M. Sasaki, *Gravitational wave constraints on the primordial black hole dominated early universe*, *JCAP* **04** (2021) 062, [[arXiv:2012.08151](#)]. [Erratum: *JCAP* **11**, E01 (2021)].
 - [111] G. Domènech, V. Takhistov, and M. Sasaki, *Exploring evaporating primordial black holes with gravitational waves*, *Phys. Lett. B* **823** (2021) 136722, [[arXiv:2105.06816](#)].
 - [112] T. Papanikolaou, V. Vennin, and D. Langlois, *Gravitational waves from a universe filled with primordial black holes*, *JCAP* **03** (2021) 053, [[arXiv:2010.11573](#)].
 - [113] T. Papanikolaou, *Gravitational waves induced from primordial black hole fluctuations: the effect of an extended mass function*, *JCAP* **10** (2022) 089, [[arXiv:2207.11041](#)].
 - [114] J. H. MacGibbon, *Quark and gluon jet emission from primordial black holes. 2. The Lifetime emission*, *Phys. Rev. D* **44** (1991) 376–392.
 - [115] D. N. Page, *Particle Emission Rates from a Black Hole: Massless Particles from an Uncharged, Nonrotating Hole*, *Phys. Rev. D* **13** (1976) 198–206.
 - [116] D. N. Page, *Particle Emission Rates from a Black Hole. 2. Massless Particles from a Rotating Hole*, *Phys. Rev. D* **14** (1976) 3260–3273.
 - [117] J. H. MacGibbon and B. R. Webber, *Quark and gluon jet emission from primordial black holes: The instantaneous spectra*, *Phys. Rev. D* **41** (1990) 3052–3079.
 - [118] A. Cheek, L. Heurtier, Y. F. Perez-Gonzalez, and J. Turner, *Redshift effects in particle production from Kerr primordial black holes*, *Phys. Rev. D* **106** (2022), no. 10 103012, [[arXiv:2207.09462](#)].
 - [119] A. Arbey and J. Auffinger, *BlackHawk: A public code for calculating the Hawking evaporation spectra of any black hole distribution*, *Eur. Phys. J. C* **79** (2019), no. 8 693, [[arXiv:1905.04268](#)].
 - [120] A. Arbey and J. Auffinger, *Physics Beyond the Standard Model with BlackHawk v2.0*, *Eur. Phys. J. C* **81** (2021) 910, [[arXiv:2108.02737](#)].
 - [121] H. Assadullahi and D. Wands, *Gravitational waves from an early matter era*, *Phys. Rev. D* **79** (2009) 083511, [[arXiv:0901.0989](#)].
 - [122] **Planck** Collaboration, Y. Akrami et al., *Planck 2018 results. X. Constraints on inflation*, *Astron. Astrophys.* **641** (2020) A10, [[arXiv:1807.06211](#)].
 - [123] E. Thrane and J. D. Romano, *Sensitivity curves for searches for gravitational-wave backgrounds*, *Phys. Rev. D* **88** (2013), no. 12 124032, [[arXiv:1310.5300](#)].
 - [124] **LIGO Scientific** Collaboration, J. Aasi et al., *Advanced LIGO*, *Class. Quant. Grav.* **32** (2015) 074001, [[arXiv:1411.4547](#)].
 - [125] **LIGO Scientific, Virgo** Collaboration, B. P. Abbott et al., *GW150914: Implications for the stochastic gravitational wave background from binary black holes*, *Phys. Rev. Lett.* **116** (2016), no. 13 131102, [[arXiv:1602.03847](#)].
 - [126] G. Janssen et al., *Gravitational wave astronomy with the SKA*, *PoS AASKA14* (2015) 037, [[arXiv:1501.00127](#)].
 - [127] N. Bartolo et al., *Science with the space-based interferometer LISA. IV: Probing inflation with gravitational waves*, *JCAP* **12** (2016) 026, [[arXiv:1610.06481](#)].
 - [128] P. Auclair et al., *Cosmology with the Laser Interferometer Space Antenna*, [arXiv:2204.05434](#).

- [129] L. Badurina, O. Buchmueller, J. Ellis, M. Lewicki, C. McCabe, and V. Vaskonen, *Prospective sensitivities of atom interferometers to gravitational waves and ultralight dark matter*, *Phil. Trans. A. Math. Phys. Eng. Sci.* **380** (2021), no. 2216 20210060, [[arXiv:2108.02468](#)].
- [130] **AEDGE** Collaboration, Y. A. El-Neaj et al., *AEDGE: Atomic Experiment for Dark Matter and Gravity Exploration in Space*, *EPJ Quant. Technol.* **7** (2020) 6, [[arXiv:1908.00802](#)].
- [131] L. Badurina et al., *AION: An Atom Interferometer Observatory and Network*, *JCAP* **05** (2020) 011, [[arXiv:1911.11755](#)].
- [132] P. W. Graham, J. M. Hogan, M. A. Kasevich, and S. Rajendran, *Resonant mode for gravitational wave detectors based on atom interferometry*, *Phys. Rev. D* **94** (2016), no. 10 104022, [[arXiv:1606.01860](#)].
- [133] **MAGIS** Collaboration, P. W. Graham, J. M. Hogan, M. A. Kasevich, S. Rajendran, and R. W. Romani, *Mid-band gravitational wave detection with precision atomic sensors*, [arXiv:1711.02225](#).
- [134] M. Punturo et al., *The Einstein Telescope: A third-generation gravitational wave observatory*, *Class. Quant. Grav.* **27** (2010) 194002.
- [135] S. Hild et al., *Sensitivity Studies for Third-Generation Gravitational Wave Observatories*, *Class. Quant. Grav.* **28** (2011) 094013, [[arXiv:1012.0908](#)].
- [136] K. Yagi and N. Seto, *Detector configuration of DECIGO/BBO and identification of cosmological neutron-star binaries*, *Phys. Rev. D* **83** (2011) 044011, [[arXiv:1101.3940](#)]. [Erratum: *Phys.Rev.D* 95, 109901 (2017)].
- [137] J. Crowder and N. J. Cornish, *Beyond LISA: Exploring future gravitational wave missions*, *Phys. Rev. D* **72** (2005) 083005, [[gr-qc/0506015](#)].
- [138] A. Sesana et al., *Unveiling the gravitational universe at μ -Hz frequencies*, *Exper. Astron.* **51** (2021), no. 3 1333–1383, [[arXiv:1908.11391](#)].
- [139] J. Garcia-Bellido, H. Murayama, and G. White, *Exploring the early Universe with Gaia and Theia*, *JCAP* **12** (2021), no. 12 023, [[arXiv:2104.04778](#)].
- [140] **NANOGrav** Collaboration, Z. Arzoumanian et al., *The NANOGrav 12.5 yr Data Set: Search for an Isotropic Stochastic Gravitational-wave Background*, *Astrophys. J. Lett.* **905** (2020), no. 2 L34, [[arXiv:2009.04496](#)].
- [141] B. Goncharov et al., *On the Evidence for a Common-spectrum Process in the Search for the Nanohertz Gravitational-wave Background with the Parkes Pulsar Timing Array*, *Astrophys. J. Lett.* **917** (2021), no. 2 L19, [[arXiv:2107.12112](#)].
- [142] S. Chen et al., *Common-red-signal analysis with 24-yr high-precision timing of the European Pulsar Timing Array: inferences in the stochastic gravitational-wave background search*, *Mon. Not. Roy. Astron. Soc.* **508** (2021), no. 4 4970–4993, [[arXiv:2110.13184](#)].
- [143] J. Antoniadis et al., *The International Pulsar Timing Array second data release: Search for an isotropic gravitational wave background*, *Mon. Not. Roy. Astron. Soc.* **510** (2022), no. 4 4873–4887, [[arXiv:2201.03980](#)].
- [144] D. Hooper, G. Krnjaic, J. March-Russell, S. D. McDermott, and R. Petrossian-Byrne, *Hot Gravitons and Gravitational Waves From Kerr Black Holes in the Early Universe*, [arXiv:2004.00618](#).
- [145] **Planck** Collaboration, N. Aghanim et al., *Planck 2018 results. VI. Cosmological parameters*, *Astron. Astrophys.* **641** (2020) A6, [[arXiv:1807.06209](#)]. [Erratum: *Astron.Astrophys.* 652, C4 (2021)].
- [146] **CMB-HD** Collaboration, S. Aiola et al., *Snowmass2021 CMB-HD White Paper*, [arXiv:2203.05728](#).

- [147] **CMB-Bharat** Collaboration, <http://cmb-bharat.in>.
- [148] **CMB-S4** Collaboration, K. Abazajian et al., *Snowmass 2021 CMB-S4 White Paper*, [arXiv:2203.08024](https://arxiv.org/abs/2203.08024).
- [149] S. Henrot-Versille et al., *Improved constraint on the primordial gravitational-wave density using recent cosmological data and its impact on cosmic string models*, *Class. Quant. Grav.* **32** (2015), no. 4 045003, [[arXiv:1408.5299](https://arxiv.org/abs/1408.5299)].
- [150] T. L. Smith, E. Pierpaoli, and M. Kamionkowski, *A new cosmic microwave background constraint to primordial gravitational waves*, *Phys. Rev. Lett.* **97** (2006) 021301, [[astro-ph/0603144](https://arxiv.org/abs/astro-ph/0603144)].
- [151] **Planck** Collaboration, P. A. R. Ade et al., *Planck 2015 results. XIII. Cosmological parameters*, *Astron. Astrophys.* **594** (2016) A13, [[arXiv:1502.01589](https://arxiv.org/abs/1502.01589)].
- [152] J. Alvey, N. Sabti, M. Escudero, and M. Fairbairn, *Improved BBN Constraints on the Variation of the Gravitational Constant*, *Eur. Phys. J. C* **80** (2020), no. 2 148, [[arXiv:1910.10730](https://arxiv.org/abs/1910.10730)].
- [153] **Particle Data Group** Collaboration, M. Tanabashi et al., *Review of Particle Physics*, *Phys. Rev. D* **98** (2018), no. 3 030001.
- [154] **Super-Kamiokande** Collaboration, K. Abe et al., *Search for proton decay via $p \rightarrow e^+ \pi^0$ and $p \rightarrow \mu^+ \pi^0$ in 0.31 megaton-years exposure of the Super-Kamiokande water Cherenkov detector*, *Phys. Rev. D* **95** (2017), no. 1 012004, [[arXiv:1610.03597](https://arxiv.org/abs/1610.03597)].
- [155] T. C. Gehrman, B. Shams Es Haghi, K. Sinha, and T. Xu, *Baryogenesis, Primordial Black Holes and MHz-GHz Gravitational Waves*, [arXiv:2211.08431](https://arxiv.org/abs/2211.08431).
- [156] N. Bhaumik and R. K. Jain, *Small scale induced gravitational waves from primordial black holes, a stringent lower mass bound, and the imprints of an early matter to radiation transition*, *Phys. Rev. D* **104** (2021), no. 2 023531, [[arXiv:2009.10424](https://arxiv.org/abs/2009.10424)].